Cell Reports
Medicine

Article

Mediator complex subunit 1 architects a tumorigenic Treg cell program independent of inflammation

Graphical abstract

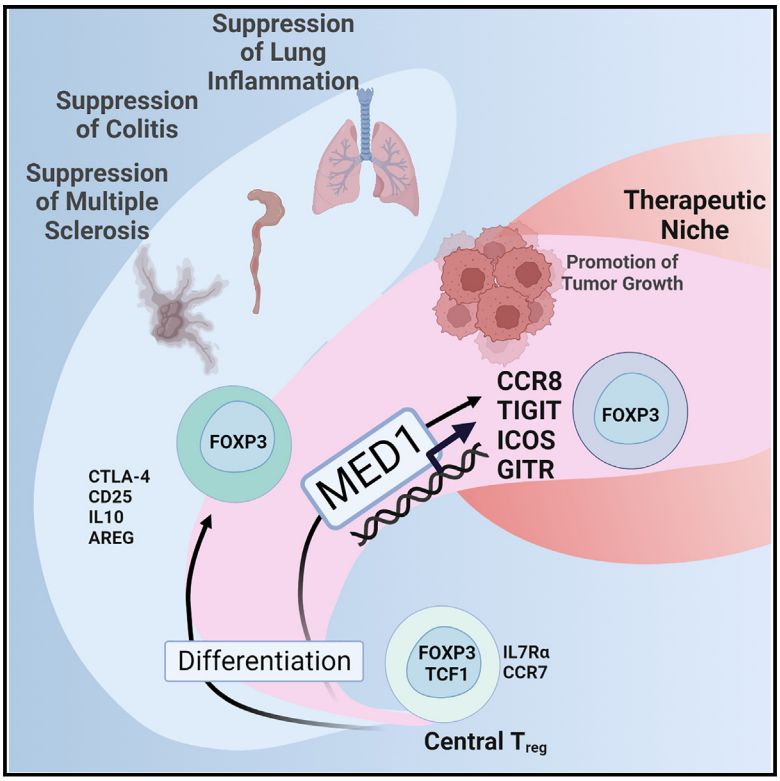

Highlights

- T_{reg} MED1 deletion enhances antitumor immunity without autoimmune inflammation
- MED1 promotes tumor-specific differentiation and suppressive functions of T_{reg} cells
- MED1 controls effector T_{reg} gene expression independent of chromatin accessibility
- Tumors and non-malignant inflammation promote divergent paths of T_{reg} differentiation

Authors

Shuvam M. Chaudhuri, Samuel E. Weinberg, Dongmei Wang, ..., Ronen Sumagin, Yana Zhang, Deyu Fang

Correspondence

fangd@northwestern.edu

In brief

Chaudhuri et al. uncover unique paths of differentiation for T regulatory cells between malignant and non-malignant inflammation, which are regulated by mediator complex subunit 1. These findings provide evidence for an immunotherapeutic niche for targeting T regulatory cells.

Chaudhuri et al., 2024, Cell Reports Medicine 5, 101441
March 19, 2024
https://doi.org/10.1016/j.xcrm.2024.101441

CellPress

Cell Reports Medicine

CellPress
OPEN ACCESS

Article

Mediator complex subunit 1 architects a tumorigenic Treg cell program independent of inflammation

Shuvam M. Chaudhuri,[1] Samuel E. Weinberg,[1] Dongmei Wang,[1,2] Lenore K. Yalom,[1] Elena Montauti,[1,7] Radhika Iyer,[1] Amy Y. Tang,[1] Manuel A. Torres Acosta,[3,4] Jian Shen,[1] Nikita L. Mani,[1] Shengnan Wang,[1] Kun Liu,[1] Weiyuan Lu,[1] Triet M. Bui,[1,8] Laura D. Manzanares,[1] Zeinab Dehghani,[1] Ching Man Wai,[5,6] Beixue Gao,[1] Juncheng Wei,[1] Feng Yue,[1,2,6] Weiguo Cui,[1] Benjamin D. Singer,[3,6] Ronen Sumagin,[1,7] Yana Zhang,[1,9] and Deyu Fang[1,2,10,*]

[1]Department of Pathology, Feinberg School of Medicine, Northwestern University, Chicago, IL 60611, USA
[2]Robert H. Lurie Comprehensive Cancer Center, Feinberg School of Medicine, Northwestern University, Chicago, IL 60611, USA
[3]Division of Pulmonary and Critical Care Medicine, Feinberg School of Medicine, Northwestern University, Chicago, IL 60611, USA
[4]Medical Scientist Training Program, Feinberg School of Medicine, Northwestern University, Chicago, IL 60611, USA
[5]Center for Genetic Medicine, Feinberg School of Medicine, Northwestern University, Chicago, IL 60611, USA
[6]Department of Biochemistry and Molecular Genetics, Feinberg School of Medicine, Northwestern University, Chicago, IL 60611, USA
[7]Present address: Division of Hematology/Oncology, Department of Medicine, University of California, San Francisco, San Francisco, CA 94143, USA
[8]Present address: Department of Medical Oncology, Dana-Farber Cancer Institute, 450 Brookline Ave, Boston, MA 02215, USA
[9]Present address: Department of Otorhinolaryngology-Head and Neck Surgery, The Third Affiliated Hospital of Sun Yat-sen University, Guangzhou 510630, China
[10]Lead contact
*Correspondence: fangd@northwestern.edu
https://doi.org/10.1016/j.xcrm.2024.101441

SUMMARY

While immunotherapy has revolutionized cancer treatment, its safety has been hampered by immunotherapy-related adverse events. Unexpectedly, we show that Mediator complex subunit 1 (MED1) is required for T regulatory (T_{reg}) cell function specifically in the tumor microenvironment. T_{reg} cell-specific MED1 deletion does not predispose mice to autoimmunity or excessive inflammation. In contrast, MED1 is required for T_{reg} cell promotion of tumor growth because MED1 is required for the terminal differentiation of effector T_{reg} cells in the tumor. Suppression of these terminally differentiated T_{reg} cells is sufficient for eliciting antitumor immunity. Both human and murine T_{reg} cells experience divergent paths of differentiation in tumors and matched tissues with non-malignant inflammation. Collectively, we identify a pathway promoting the differentiation of a T_{reg} cell effector subset specific to tumors and demonstrate that suppression of a subset of T_{reg} cells is sufficient for promoting antitumor immunity in the absence of autoimmune consequences.

INTRODUCTION

T regulatory (T_{reg}) cells are a subset of immunosuppressive $CD4^+$ T cells, defined by expression of the transcription factor FOXP3, that are critical for maintaining immune homeostasis.[1–3] Importantly, T_{reg} cell infiltration and suppressive function in tumors, especially when enhanced relative to $CD8^+$ T cell infiltration, is prognostic of poor outcomes in patients across various tumor types.[4–8] T_{reg} cells are thought to promote tumor growth through a variety of mechanisms. These include the production of immunosuppressive cytokines (IL-10, IL-35, and transforming growth factor β),[9,10] modulation of their microenvironment (CD25, CD39, and CD73),[11] cytotoxic function (granzymes and perforin), immune-inhibitory molecules (CTLA-4 and programmed cell death 1 [PD-1]),[12,13] and expression of growth factors and ligands (amphiregulin, neuropilin-1, and others).[14,15] It is not well understood whether all T_{reg} cells exercise all these functions or whether heterogeneous populations of T_{reg} cells use discrete, tumor-promoting functions.

While targeting T_{reg} cells presents a reasonable immunotherapeutic strategy for cancer, it is currently challenging to target the lineage-determining transcription factor FOXP3. Moreover, this approach is unfavorable because systemic depletion of T_{reg} cells leads to deleterious autoimmunity.[16] Current immunotherapies, such as CTLA-4 and PD-1 targeted checkpoint blockade, have experienced success but are often accompanied by severe immune-related adverse events (irAEs) that can necessitate cessation of therapy.[17–20] PD-1 blockade has even been shown to amplify T_{reg} cell function and enhance the hyper-progression of tumors in some cases.[20] These issues highlight the need to identify alternative tumor-specific nodes for diminishing tumor immunosuppression without eliciting irAEs.

Prior work has demonstrated that T_{reg} cells in tumors have increased expression of an immunosuppressive program relative

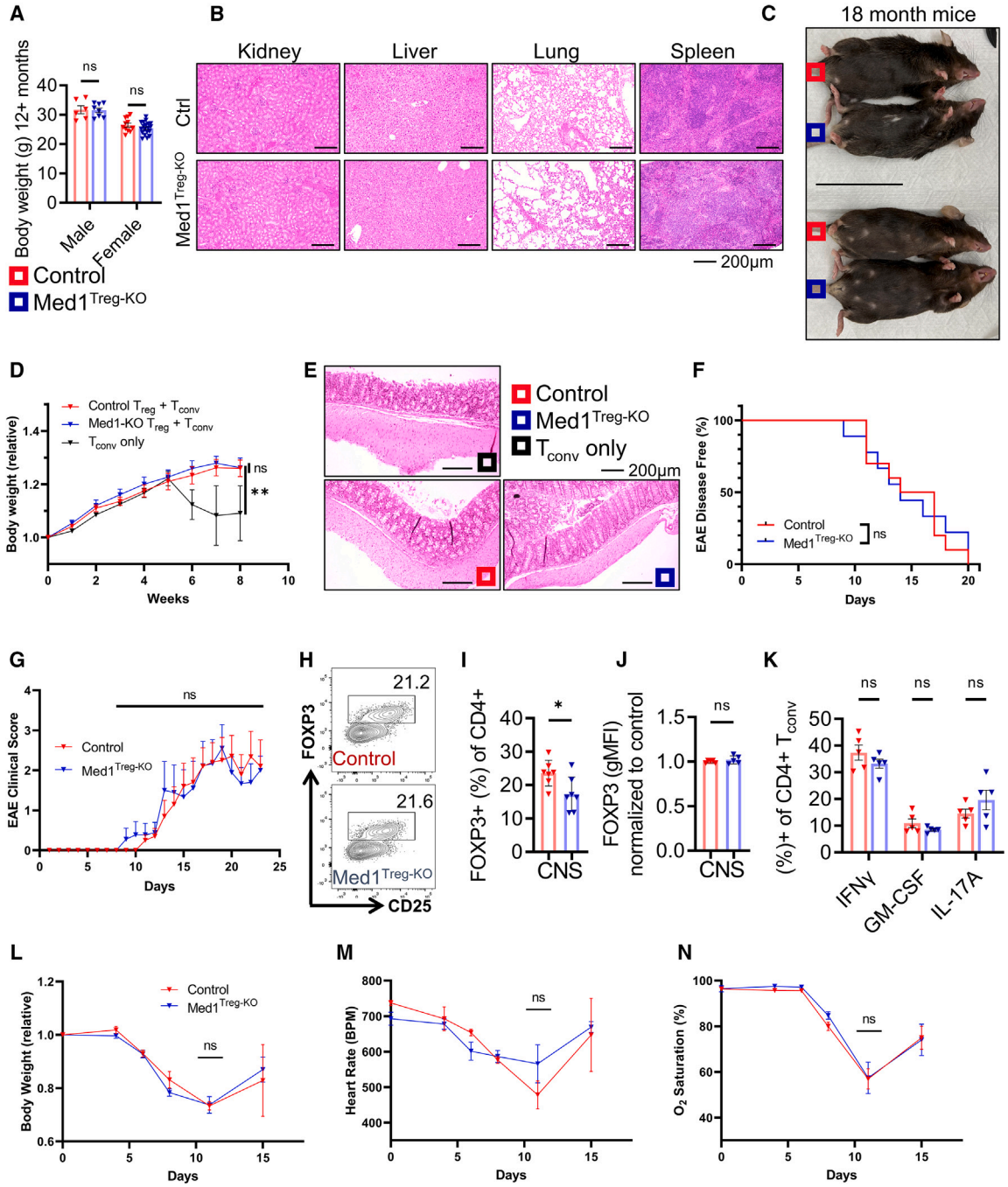

Figure 1. MED1 is dispensable for T_{reg} cell function across inflammatory contexts

(A) *Foxp3*$^{YFP-cre}$ (control) and *Foxp3*$^{YFP-cre}$/*Med1*$^{fl/fl}$ (Med1$^{Treg-KO}$) mice were aged to 12–14 months and bodyweights were measured. (n = 611 for control and n = 819 for Med1$^{Treg-KO}$ for male and female, respectively.)

(B) Representative hematoxylin and eosin (H&E) staining from organs of mice in (A).

(C) Representative photograph of mice aged to 18 months.

(D) CD45.1 CD4$^+$ T_{conv} cells were either transferred in alone or with T_{reg} cells isolated from control or Med1$^{Treg-KO}$ mice to induce colitis. Body weight displayed relative to start (n = 5 per group).

(E) Representative H&E staining from colons of mice in (D).

(F)EAE was induced by immunization with MOG peptide. Disease incidence was tracked per group during experiment.

(G) Clinical scores measured during EAE (n = 10 control and n = 9 Med1$^{Treg-KO}$).

(H) Representative flow plots of FOXP3 expression of CD4 T cells within the CNS.

(I) Summary of (H) (n = 7 control and n = 7 Med1$^{Treg-KO}$).

(legend continued on next page)

to the periphery.[5,21–25] These programs are similarly enhanced in tissues relative to the periphery and are regulated by transcription factors BATF, IRF4, and FOXM1.[21,22,26,27] Whether T_{reg} cells in tumors acquire effector programs relative to tissues is largely unknown.

Unexpectedly, we discovered that MED1 promotes the differentiation and function of a discrete tumor-supportive population of T_{reg} cells and, thus, presents a node for designing specific immunotherapies. MED1 is a subunit of the Mediator complex, which transduces signals from transcription factors to the RNA polymerase II complex to drive transcription.[28–32] MED1 has been shown to be important for specific developmental and differentiation processes including adipocyte development, invariant natural killer T (iNKT) cell development, and luminal cell differentiation.[33–35] Because MED1 regulates discrete differentiation processes at the transcriptional level, and, more important, we have identified MED1 as an interacting protein of USP22, a deubiquitinase critical for T_{reg} cell functions,[36] we hypothesized that MED1 may be critical for a tumor specific T_{reg} cell differentiation path or function. Indeed, CRISPR screens performed by our laboratory have suggested Mediator complex subunits may be important in regulating T_{reg} cell functions.[37] While the majority of Mediator complex subunits are required for Mediator complex function, and by extension cellular viability, MED1 is a non-essential subunit,[38] thus enabling us to study it in T_{reg} cells. Importantly, the role of MED1 or the Mediator complex in regulating T_{reg} cell function has never been described.

Surprisingly, MED1 is dispensable for normal T_{reg} cell development, maintenance, and function, as well as control of inflammation stemming from colitis, experimental autoimmune encephalomyelitis (EAE), or influenza. At the molecular level, MED1 is dispensable for regulating chromatin accessibility of intratumoral T_{reg} cells, but required for transcription of a tumor T_{reg} cell effector program associated with transcription factors BATF, IRF4, FOS, and JUN. Finally, analysis of murine and human T_{reg} cells isolated from tumors and matched inflamed but non-malignant tissue revealed distinct differentiation of T_{reg} cell populations. These findings highlight that a differentiated, tumor-specific T_{reg} cell population is present in various cancers and may be targeted to elicit antitumor immunity without risking autoimmunity.

RESULTS

MED1 is dispensable for T_{reg} cell maintenance of immune system homeostasis

To elucidate MED1's control of T_{reg} cell function, we generated T_{reg} cell-specific MED1 knockout mice ($Med1^{Treg-KO}$) by crossing $Foxp3^{YFP-Cre}$ mice with $Med1^{fl/fl}$ mice.[39] Where $Med1^{Treg-KO}$ mice are shown, $Foxp3^{YFP-Cre}$ mice are used as controls. We confirmed efficient, T_{reg} cell-specific deletion of MED1 by western blot (Figure S1A). $Med1^{Treg-KO}$ animals demonstrated normal thymocyte development, similar T_{reg} cell proportions in peripheral lymphoid organs and similar FOXP3 levels (Figures S1B–S1G).

Deletion of MED1 did not alter CD44 and CD62L expression in the $CD8^+$ T cell compartment (Figures S1H–S1I). $CD4^+$ $FOXP3^-$ T conventional (T_{conv}) cells in spleens demonstrated a small increase in the $CD44^{hi}$ $CD62L^{lo}$ compartment (Figure S1J). The total number of splenocytes was comparable between control and $Med1^{Treg-KO}$ mice (Figure S1K). Interestingly $Med1^{Treg-KO}$ mice showed slightly higher proportions of $CD44^{hi}$ $CD62L^{lo}$ T_{reg} cells[40] in some peripheral lymphoid organs (Figure S1L). The small increase in proportion of $CD44^{hi}$ $CD62L^{lo}$ $CD4^+$ $FOXP3^-$ T_{conv} cells may be due to reported leakiness among $CD4^+$ T cells in Cre recombinase expression under control of the *Foxp3* promoter.[41]

We directly tested the suppressive function of control and MED1-deficient T_{reg} cells through an *in vitro* T_{reg} cell-suppressive assay (Figures S1M–S1N) and found no differences.[42] Last, we subjected control and MED1-deficient T_{reg} cells to genome wide bulk RNA sequencing. We found no differences in several molecules with reported functions in T_{reg} cells including *Ctla4*, *Il2ra*(CD25), and *Foxp3*, but with a modest decrease in *Il10* expression (Figure S1O). However, IL-10 expression by T_{reg} cells has been shown to be dispensable for control of systemic autoimmunity[43] and its modest reduction appears to be insufficient to impair T_{reg} ability to control adoptive transfer-induced colitis in RAG1-deficent mice. These results indicate that MED1 is dispensable for T_{reg} cell functions in immune homeostasis.

MED1 is dispensable for T_{reg} cell function across multiple inflammatory contexts

T_{reg} cell function is essential for suppressing autoimmunity and limiting tissue injury during infection (Figure S2A).[20,44–50] In addition, mice with defects in T_{reg} cell function are expected to show signs of visible inflammation as they age.[51] We aged $Med1^{Treg-KO}$ mice and control mice to 52–60 weeks of age and found no difference in bodyweight between $Med1^{Treg-KO}$ and control mice, no abnormal lymphocyte infiltration, and no evidence of systemic inflammatory disorder (Figures 1A and 1B), indicating that MED1 is not essential for suppressing aging-related inflammation at least to the age of 14 months. Prior work indicates that, if IL-10 expression was severely compromised in T_{reg} cells, this would be evident by lung inflammation by this point.[43] Mice displayed no outward signs of inflammatory disorder, such as hunched posture, even at 18 months of age (Figure 1C).

To further investigate the role of T_{reg} cell-intrinsic MED1 in maintaining immune homeostasis, we used a model of T cell

(J) FOXP3 protein expression in $CD4^+$ $FOXP3^+$ $CD25^+$ T cells in the CNS. Values are normalized to controls. (n = 5 control and n = 5 $Med1^{Treg-KO}$.)
(K) Percentage of cytokine producing $CD4^+$ FOXP3- Tconv cells in the CNS. (n = 5 control and n = 5 $Med1^{Treg-KO}$).
(L) Mice were inoculated with influenza virus and monitored over course of disease. Body weight relative to starting (n = 8 controls and n = 6 $Med1^{Treg-KO}$).
(M) Heart rate measured in beats per minute (BPM) (n = 8 controls and n = 6 $Med1^{Treg-KO}$).
(N) Oxygen saturation was measured by pulse oximeter (n = 8 controls and n = 6 $Med1^{Treg-KO}$). (A), (D), and (K) used two-way ANOVA with multiple comparisons. (F), (G), (I), (J), and (L–N) use unpaired two-tailed Student's t test at experiment conclusion. Bars represent ± SEM. Points on graph represent individual mice. (*$p < 0.05$, **$p < 0.01$.) Related to Figures S1 and S2.

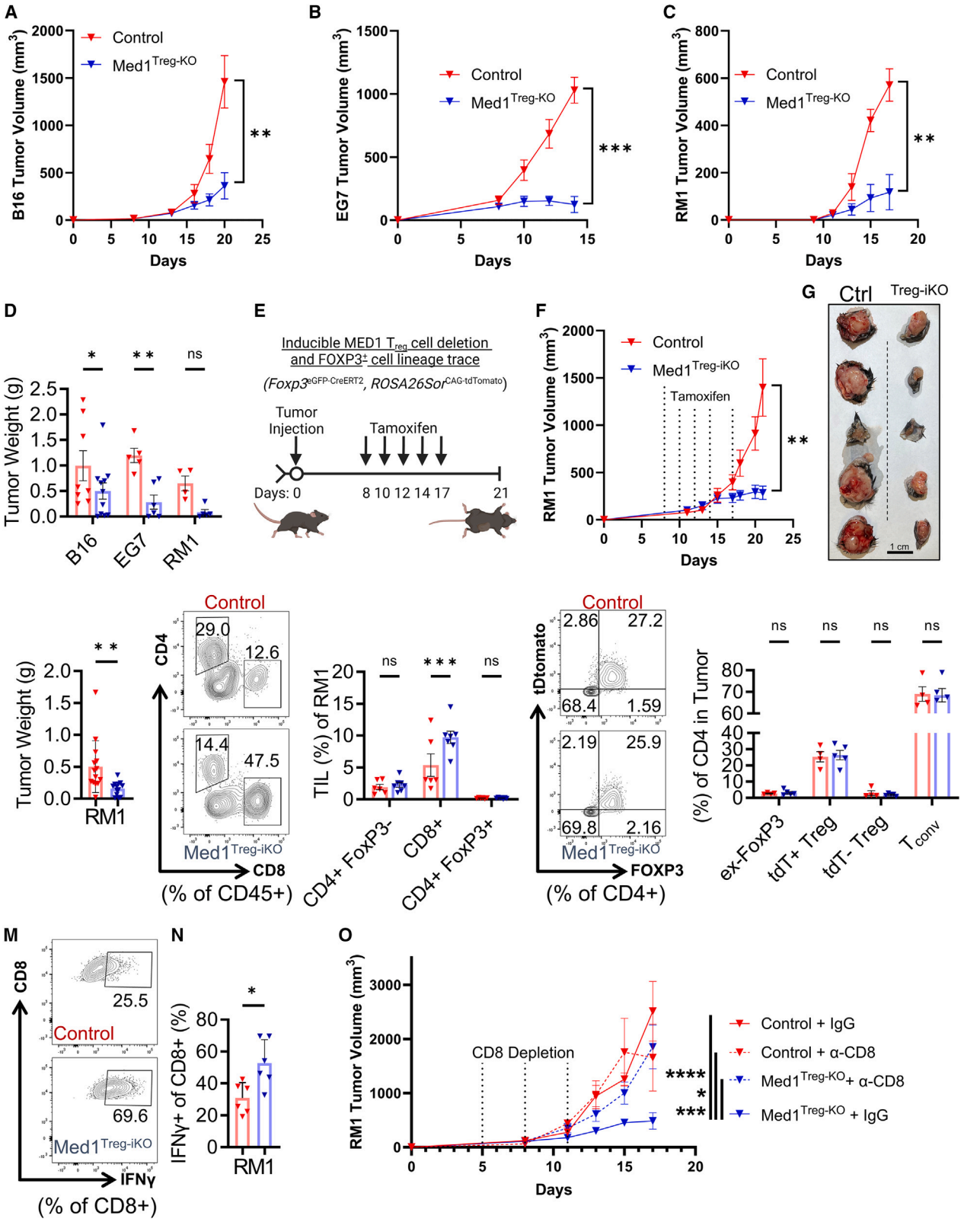

(legend on next page)

transfer mediated colitis.[52] MED1-deficient and MED1-sufficient CD45.2$^+$ T_{reg} cells achieved comparable efficacy in suppressing CD45.1$^+$ CD4$^+$ T_{conv} cell-induced colitis (Figures 1D and 1E). This is evident in that CD45.1$^+$ T_{conv} cell transfer alone caused colitis symptoms, including body weight loss and colonic inflammation (Figures 1D and 1E). Further analysis of mesenteric lymph node T cells revealed that the production of inflammatory cytokines interferon (IFN)-γ and IL17A by CD45.1$^+$ T_{conv} cells was comparable between mice receiving T_{reg} cells from either control or Med1$^{Treg-KO}$ mice (Figure S2B). Additionally, CD45.2$^+$ T_{reg} cells from control or Med1$^{Treg-KO}$ mice showed a similar ability to retain FOXP3 expression, demonstrating that MED1 deficiency does not impair T_{reg} cell lineage stability (Figure S2C), which has been shown to possibly be pathogenic in some human autoimmune conditions.[53] These data suggest that MED1 is not required for T_{reg} cell functions in protection from adoptive transfer T_{conv} cell-mediated colitis or maintenance of T_{reg} cell stability.

We next sought to define the contribution of MED1 to T_{reg} cell function in orthogonal settings of inflammation with an EAE model of multiple sclerosis.[54,55] We found no differences in disease incidence or clinical score between control and Med1$^{Treg-KO}$ mice (Figures 1F and 1G). Although there was a slight decrease in T_{reg} cell infiltration in the CNS, there were no differences in T_{reg} cell expression of FOXP3, or CD4$^+$ T_{conv} cell and CD8$^+$ T cell production of inflammatory cytokines (Figures 1H–1K, S2D–S2G). Additionally, we observed no increase in inflammatory cytokine production between T_{reg} cells from control and Med1$^{Treg-KO}$ mice demonstrating deletion of MED1 does not skew T_{reg} cells toward a pathogenic phenotype (Figure S2H).[56]

Finally, to test the recently described tissue protective role T_{reg} cells,[14,50] we challenged control and Med1$^{Treg-KO}$ mice with influenza virus. Med1$^{Treg-KO}$ animals showed similar weight loss and alterations in arterial O_2 saturation compared to control animals (Figures 1L–1N). This indicates that MED1 is dispensable for T_{reg} cell maintenance of body weight and respiratory function during influenza infection.

Collectively, these data demonstrate that MED1 is largely dispensable for T_{reg} cell function in homeostatic settings, acute models of inflammation across tissues, and lung tissue protection during influenza infection. While many T_{reg} cell functions are commonly used in homeostatic, autoimmune inflammatory conditions, infections, and tumor microenvironments, our data indicate that MED1 may control tumor-specific function of T_{reg} cells.

MED1 is required for T_{reg} cell suppression of tumor growth in a CD8$^+$ T cell-dependent manner but not intratumoral T_{reg} cell accumulation

In contrast with homeostatic and non-malignant inflammatory conditions, we found that T_{reg} cell-specific deletion of MED1 resulted in reduced tumor volume and weight in syngeneic models of B16 melanoma, EG7 lymphoma, and RM1 prostate cancer (Figures 2A–2D), demonstrating that MED1 is specifically required for T_{reg} cell promotion of tumor growth. Next, we sought to understand whether T_{reg} cells were unable to accumulate in tumors, or whether their function was compromised within tumors. MED1 deletion did not affect T_{reg} cell accumulation and FOXP3 expression in tumors, as T_{reg} cells comprised similar proportions of live cells across conditions and tumor models (Figures S3A–S3F). Despite equal T_{reg} cell accumulation and FOXP3 expression, CD8$^+$ T cell infiltration was significantly increased in tumors grown in Med1$^{Treg-KO}$ animals (Figures S3D–S3I). Additionally, IFN-γ secretion was slightly increased in RM1 tumor-infiltrating CD8$^+$ T cells (Figures S3J–S3K). These data suggest that MED1, independent of FOXP3 expression, is crucial for T_{reg} cell-mediated suppression of CD8$^+$ T cell infiltration in tumors.

To further investigate the role of MED1 in suppressing established tumor growth, we bred *Med1*$^{fl/fl}$ animals with mice harboring *Foxp3*$^{eGFP-CreERT2}$ and *ROSA26*$^{SorCAG-tdTomato}$ alleles (Med1$^{Treg-iKO}$). This allows inducible MED1 deletion in T_{reg} cells and lineage tracing of all FOXP3$^+$ cells (Figures 2E and S4A). In experiments using Med1$^{Treg-IKO}$ mice, control mice were

Figure 2. MED1 is required for T_{reg} cell promotion of tumor growth

(A) B16 tumors were implanted into flanks of *Foxp3*$^{YFP-cre}$ (controls) and *Foxp3*$^{YFP-cre}$/*Med1*$^{fl/fl}$ (Med1$^{Treg-KO}$) mice between 8 and 16 weeks of age. and measured for volume. (n = 12 control and n = 11 Med1$^{Treg-KO}$).

(B) EG7 tumors were implanted into flanks and measured for volume. (n = 5 control and n = 6 Med1$^{Treg-KO}$.)

(C) RM1 tumors were implanted into flanks and measured for volume. (n = 4 controls and n = 5 Med1$^{Treg-KO}$.)

(D) Tumor weights from B16, EG7, and RM1 tumors. (Respectively, for B16, EG7, and RM1 tumors: n = 8, 5, and 4 for controls and n = 11, 6, ad 5 for Med1$^{Treg-KO}$.)

(E) Experimental setup for tumor experiments using *Foxp3*$^{eGFP-CreERT2}$, *ROSA26Sor*$^{CAG-tdTomato}$ (control) *Med1*^{fl}, *Foxp3*$^{eGFP-CreERT2}$, and *ROSA26Sor*$^{CAG-tdTomato}$ (Med1$^{Treg-iKO}$) with inducible MED1 deletion and FOXP3 lineage trace.

(F) RM1 tumors were implanted into flanks and measured for volume. (n = 14 controls and n = 13 Med1$^{Treg-iKO}$.)

(G) Representative photograph of RM1 tumors.

(H) Tumor weights from RM1 tumors (n = 14 controls and n = 13 Med1$^{Treg-iKO}$).

(I) Representative flow plots of CD4 and CD8 expression within the CD45$^+$ cells within RM1 tumors.

(J) CD45$^+$ CD3ε^+ CD4$^+$ FOXP3$^-$, CD45$^+$ CD3ε+ CD8$^+$, and of CD45$^+$ CD3ε^+ CD4$^+$ FOXP3$^+$ T cells proportion of total live cells from RM1 tumors (n = 6 controls and n = 7 Med1$^{Treg-iKO}$).

(K) Representative flow plots of T_{conv} (FoxP3$^-$ tdTomato$^-$), ex-FOXP3 (FOXP3$^-$ tdTomato$^+$), tdT$^+$ T_{reg} (FOXP3$^+$ tdTomato$^+$), tdT$^-$ T_{reg} (FOXP3$^+$ tdTomato$^+$) within the intratumoral CD4$^+$ T cell compartment.

(L) Summary data of (K) (n = 4 controls and n = 5 Med1$^{Treg-iKO}$).

(M) Representative flow plots of IFN-γ production within intratumoral CD8$^+$ T cell compartment.

(N) Summary data of M (n = 6 controls and n = 6 Med1$^{Treg-iKO}$).

(O) RM1 tumors were implanted in mice. IgG control or α-CD8 depleting antibody treatment started on day 5. (n = 4 for each group.) (A–C), (F), (H), and (Q–T) use unpaired Student two-tailed t test at experiment conclusion. (D), (J), (L), and (O) used two-way ANOVA with multiple comparisons. Bars represent ± SEM. Points on graph except for (S) represent individual mice. (*p < 0.05, **p < 0.01, ***p < 0.001, ****p < 0.0001.) Related to Figures S3, S4, and Table S1.

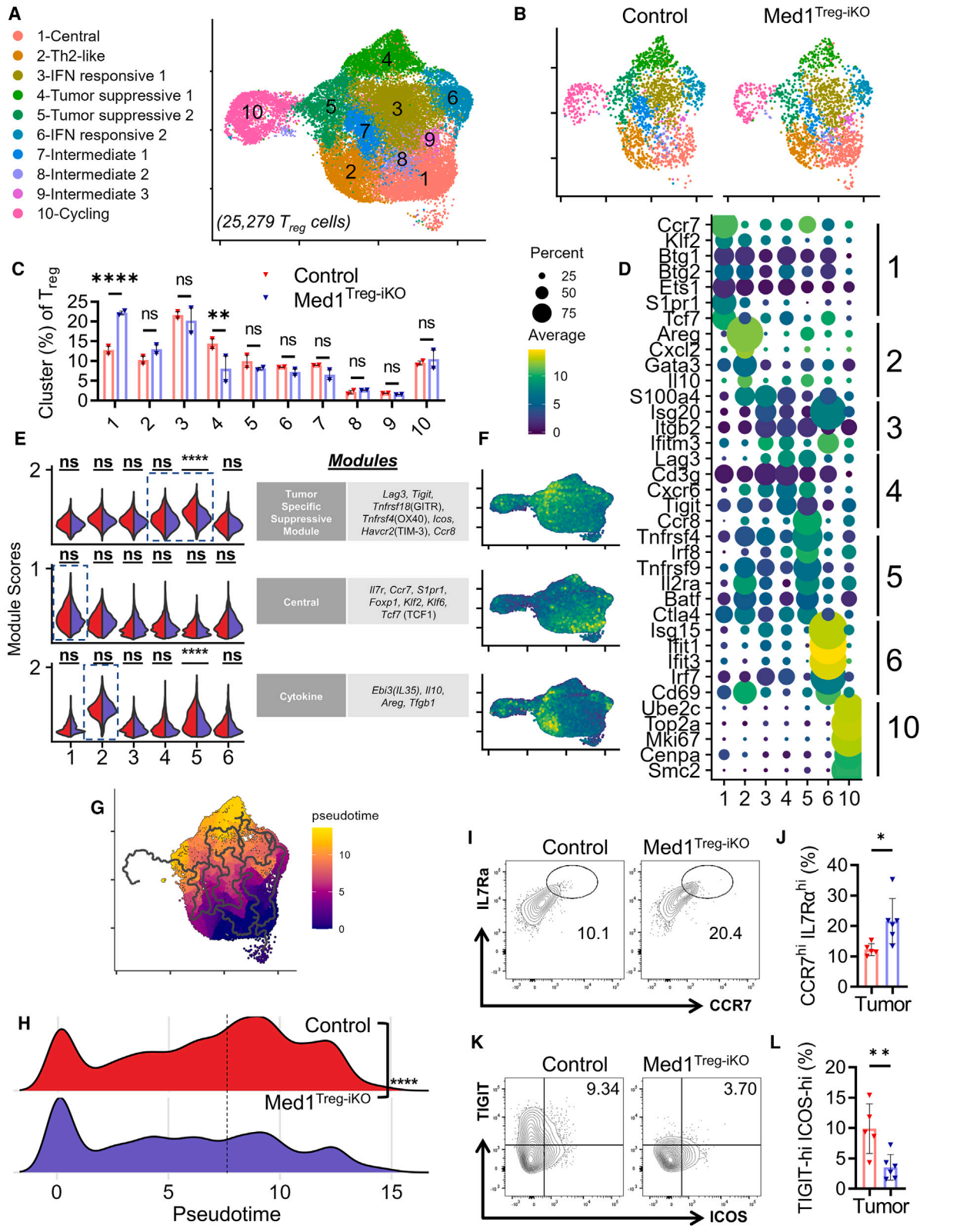

(legend on next page)

homozygous for *Foxp3*$^{eGFP-CreERT2}$ and *ROSA26Sor*$^{CAG-tdTomato}$ alleles and also administered tamoxifen. We confirmed that MED1 was efficiently and specifically deleted in CD4$^+$ tdTomato$^+$ but not tdTomato$^-$ T cells (Figures S4B and S4C), and that CD4$^+$ FOXP3$^-$ T_{conv} and CD8$^+$ T cells were not altered in naive and memory compartments by deletion of MED1 in T_{reg} cells (Figures S4D and S4E).

We then inoculated RM1 tumors in mice and administered tamoxifen to induce MED1 deletion once tumors were palpable with an average size of 50–100 mm^3 (Figure 2E). We observed that deletion of MED1 in T_{reg} cells, even after tumors were initiated, dramatically suppressed tumor growth and, to a similar extent to tumors grown in mice with constitutive T_{reg} cell-specific MED1 deletion (Figures 2F–2H). As a control, mice without tamoxifen administration showed no phenotype when inoculated with tumors (Figures S4F–S4H). We observed a significant increase in CD8$^+$ T cell infiltration in tumors, but unaltered T_{reg} cell infiltration (Figures 2I and 2J). Lineage tracing analysis revealed that the proportions of T_{conv} (FOXP3$^-$ tdTomato$^-$), ex-FOXP3 (FOXP3$^-$ tdTomato$^+$), tdT + T_{reg} (FOXP3$^+$ tdTomato$^+$), tdT$^-$ T_{reg} (FOXP3$^+$ tdTomato$^+$) within the intratumoral CD4$^+$ T cell compartment were similar, confirming that MED1 is not required for maintenance of FOXP3 expression and T_{reg} cell identity in the tumor microenvironment (Figures 2K and 2L). Despite this, CD8$^+$ T cell cytotoxic function was enhanced, as documented by increased IFN-γ production in Med1$^{Treg-iKO}$ mice (Figures 2M and 2N). While the myeloid compartments are largely comparable, we did observe a small decrease in myeloid-derived suppressor cell infiltration and a decrease in programmed cell death ligand 1 expression by tumor-associated macrophages (Figures S4I and S4J). We also found that inducible deletion of T_{reg} MED1 led to decreased EG7 tumor growth and increased granzyme B and IFN-γ production in CD8$^+$ tumor-infiltrating lymphocytes (Figures S4K–S4O). We did not see yet an obvious increase in CD8$^+$ T cell infiltration at the point of euthanasia, which may be due to kinetics of MED1 deletion and EG7 tumor progression.

These data indicate that MED1 is essential for T_{reg} cell suppression of CD8$^+$ T cell antitumor immunity, but not T_{reg} cell infiltration and FOXP3 expression in the tumor microenvironment. Supporting this conclusion, CD8$^+$ T cell depletion largely abolished the reduced RM1 tumor growth in Med1$^{Treg-KO}$ mice (Figure 2O). Collectively, these data indicate that MED1 is dispensable for T_{reg} cell trafficking and accumulation in tumors; however, it is required for T_{reg} cell-mediated suppression of antitumor immunity in a CD8$^+$ T cell-dependent manner.

MED1 promotes a specific effector T_{reg} cell differentiation program in the tumor microenvironment

Intratumoral T cells exist in several distinct functional states.[57] Because MED1 fundamentally regulates transcription during development and differentiation, we hypothesized that Med1$^{Treg-iKO}$ mice might fail to generate one or more tumor-promoting T_{reg} cell populations. We isolated T_{reg} cells from RM1 tumors in control and Med1$^{Treg-iKO}$ mice on day 15 before tumor size divergence to minimize the influence of differences in the tumor microenvironment on T_{reg} cell transcriptomes (Figures 2F and S5A). Single cell RNA sequencing of 25,279 total T_{reg} cells revealed 10 distinct clusters, supporting previous findings[57] of heterogeneous T_{reg} cell populations within tumors (Figure 3A). The identity of T_{reg} cells was confirmed by visualization of *Foxp3* and *Il2ra* expression on UMAP plots (Figure S5B). Comparison of T_{reg} cells between conditions revealed that a higher proportion MED1-deficient T_{reg} cells skewed toward cluster 1, whereas a lesser proportion skewed toward cluster 4, and frequency across other clusters was comparable (Figures 3B and 3C). Further analysis of cluster-specific markers revealed that cluster 1 was most consistent with a central like T_{reg} cell population[40] with relatively higher expression of *Klf2*, *Tcf7*, *Ccr7*, *Il7ra*, and *S1pr1* (Figures 3D and S5C). Cluster 2, T helper 2 (Th2)-like T_{reg} cells, were high in *Gata3*, *Areg*, *Il10*, *Ctla4*, and *Il2ra* expression, but showed no appreciable difference between control and Med1$^{Treg-iKO}$ mice (Figures 3C, 3D, and S5D)[58] indicating that MED1 is not essential for the generation of this Th2-like effector subset. This is consistent with the lack of phenotypes in the colitis model and influenza models, which are highly dependent on T_{reg} cell production of IL-10 and amphiregulin, respectively (Figures 1D, 1E, 1L–1N).[14,59,60] T_{reg} cells in clusters 4 and 5 were consistent with previously described tumor effector T_{reg} cell phenotypes, showing relatively high expression of *Lag3*, *Tigit*, *Ccr8*, *Tnfrsf4*, *Tnfrsf9*, and *Ctla4* (Figures 3D, S5E, and S5F).[61,62] Importantly, depletion of these subsets[63,64] or decrease of their suppressive molecules, such as

Figure 3. MED1 is essential for optimal differentiation of specific T_{reg} cell effector populations

(A) Integrated UMAP clustering of T_{reg} cells isolated from RM1 tumors.
(B) UMAP diagrams of T_{reg} cells isolated from RM1 tumors in control (9,838 cells) and Med1$^{Treg-IKO}$ mice (15,441 cells).
(C) Cluster proportion of total T_{reg} cells from condition (n = 2 biological replicates, each biological replicate contains cells pooled from 2–3 separate mice).
(D) Dot plot representing gene expression and percent expression within cells from each cluster.
(E) Module scores comparing T_{reg} cells from control and Med1$^{Treg-IKO}$ within clusters. Clusters with the highest expression of module are outlined.
(F) Module scores portrayed on UMAP plots.
(G) Pseudotime representation portrayed on integrated UMAP plot.
(H) Ridge plot depicting pseudotime by condition.
(I) Representative flow plot of CCR7 and IL7Ra expression in intratumoral T_{reg} cells.
(J) Summary data from (I) (n = 5 from controls and n = 6 Med1$^{Treg-IKO}$).
(K) Representative flow plot of TIGIT and ICOS expression in intratumoral T_{reg} cells.
(L) Summary data from (K) (n = 5 from controls and n = 6 Med1$^{Treg-IKO}$). (C) used two-way ANOVA with multiple comparisons. (D) used Wilcoxon test to find genes overrepresented in clusters, all genes displayed showed p adjusted of less than 0.05 and $\log_2$(fold change) of greater than 0.4. (E) used the Mann-Whitney test to detect differences greater than 0.1 between conditions within clusters. (H) used the Mann-Whitney test. (J) and (L) use unpaired Student two-tailed t test. (*p < 0.05, **p < 0.01, ****p < 0.0001.) Related to Figure S5.

TIGIT,[61] has been demonstrated to be sufficient for impeding tumor growth. Additionally, cluster 4 and 5 T_{reg} cells showed a high expression of *NR4A* family members (Figure S5G), suggesting recent T cell receptor engagements.[57,63]

Beyond proportional differences, we attempted to gain insight into whether the function of specific T_{reg} cell subsets was compromised by MED1 deletion. To do so, we used the module scoring function within Seurat (Figure 3E).[65] Several recent studies have identified a tumor specific T_{reg} cell signature that we used to create a tumor-specific suppressive module based on *Lag3*, *Tigit*, *Tnfrsf18*(GITR), *Tnfrsf4* (OX40), *Icos*, *Havcr2* (TIM-3), and *Ccr8* expression.[5,22,27] We found that that the tumor-specific suppressive module was most highly expressed by clusters 4 and 5. MED1-deficient T_{reg} cells had a significantly lower expression of this module in cluster 5, in addition to the reduced frequency of cluster 4 T_{reg} cells (Figures 3C–3F). We also constructed module scores for central T_{reg} cells based on *Il7r*, *Ccr7*, *S1pr1*, *Foxp1*, *Klf2*, *Klf6*, and *Tcf7* (TCF1) and cytokine production based on *Ebi3*(*IL35*), *Il10*, *Areg*, and *Tfgb1* expression. We found that the central module associated most strongly with cluster 1 and that the cytokine module associated most strongly with cluster 2 (Figures 3E and 3F). Together, these data indicate that MED1 is essential for the generation or maintenance and suppressive functions of a tumor-specific effector T_{reg} cell population in the tumor.

Due to the range of T_{reg} cell phenotypes we observed, we sought to define the potential trajectories for effector T_{reg} cell differentiation within tumors using Monocle3 (Figure 3G).[66] After ordering cells in pseudotime, central T_{reg} cells (cluster 1) were situated toward the beginning of the trajectory,[67] whereas tumor suppressive T_{reg} cells (clusters 4 and 5) represented the most differentiated cells (Figure S6H). We then observed that MED1-deficient T_{reg} cells had significantly reduced pseudotime values and thus represented less differentiated T_{reg} cells relative to MED1-sufficient T_{reg} cells (Figure 3H). These data indicate that MED1 is required for optimal terminal T_{reg} cell differentiation specifically in the tumor microenvironment, which supports our discovery of MED1-deficient T_{reg} cells being held in a central state (cluster 1), but a lesser ability to differentiate into a tumor-suppressive state (clusters 4 and 5). Indeed, genes (*Ccr7*, *Il7r*, *S1pr1*, and *Tcf7*) associated with cluster 1 and MED1-deficient T_{reg} cells had negative correlations with pseudotime whereas genes (*Icos*, *Tigit*, *Tnfrsf18*, and *Irf8*) that associated with clusters 4 and 5 had positive correlations with pseudotime (Figure S5I). To confirm that MED1-deficient T_{reg} cells experience impaired differentiation, we performed flow cytometry. Intratumoral T_{reg} cells from $Med1^{Treg\text{-}iKO}$ mice possessed a greater proportion of central-like $CCR7^{hi}$, $IL7Ra^{hi}$ T_{reg} cells and a lower proportion of effector-like $TIGIT^{hi}$, $ICOS^{hi}$ T_{reg} cells (Figures 3I–3L).

Collectively, we show that T_{reg} cells may continue to differentiate within tumors to a terminal effector T_{reg} cell population, and that MED1 is required for optimal development of a specific tumor-promoting population. Importantly, MED1 is dispensable for the generation of Th2-like effector and other T_{reg} cell subsets. This additionally supports that targeting a subset of T_{reg} cells or a subset of T_{reg} cell functions is sufficient for impeding tumor growth.

MED1 enforces transcription of T_{reg} cell effector genes independent of chromatin accessibility or transcription factor expression

The Mediator complex is an essential piece of transcription machinery that is a co-activator for transcription factors and required for RNA polymerase II-dependent transcription. While most Mediator complex subunits are required for Mediator complex function and thus cellular viability, MED1 is not.[38] We sought to understand at what level MED1 enables differentiation to an effector T_{reg} cell population, so we used a multi-faceted approach comparing chromatin accessibility, gene transcription, and protein expression between MED1-deficient and MED1-sufficient T_{reg} cells in spleens and tumors (Figures 4A and S6A). We reasoned that examining chromatin accessibility would tell us one of two things: either (1) genomic regions responsible for T_{reg} cell effector function are less accessible in $Med1^{Treg\text{-}iKO}$ or (2) MED1 is dispensable for regulating accessibility but is essential for enhancing transcription. Principal component analysis of ATAC-sequencing data revealed that the T_{reg} cell microenvironment (spleen versus tumor) played a substantially more important role (62% variance) in regulating chromatin accessibility than did MED1 (<7% variance) (Figures 4B and S6B). Additionally, differential accessibility analysis of MED1-deficient and sufficient intratumoral T_{reg} cells revealed fewer than 20 genes with significant differences in chromatin accessibility in either direction (Figure S6C). These data are consistent with prior reports of MED1 function in adipocytes, where MED1 does not regulate chromatin accessibility, but does regulate RNA polymerase II recruitment and transcription of certain genes.[33] Unfortunately, the limited number of intratumoral T_{reg} cells precludes us from testing how RNA polymerase II or specific transcription factor recruitment to the genome differs in MED1-deficient cells. We did, however, find that MED1 regulated transcription of effector T_{reg} cell genes through pseudobulk analysis of our small conditional RNA sequencing data with the MAST framework (Figures S6D–S6I).[68] Despite displaying comparable chromatin accessibility, mRNA expression of effector T_{reg} cell genes such as *Tigit* and *Tnfrsf18*(GITR), and *Icos* was significantly reduced in intratumoral MED1-deficient T_{reg} cells (Figures 4C and 4D).

We then analyzed the expression of a subset of these genes through flow cytometry of splenic and intratumoral T_{reg} cells. We found that there was elicitation of an effector program in tumors relative to spleens, but that MED1 deficiency compromised the expression of effector molecules specifically in the tumor T_{reg} cells (Figures 4E–4G). Through gene set enrichment analysis,[69] we found no significant enrichment of FOXP3 target genes, supporting the notion that effector T_{reg} cell differentiation occurs independent of FOXP3 (Figures S6H and S6I). Interestingly, we did not find differences in the expression of transcription factors (IRF4, IRF8, and HELIOS) thought to control expression of effector T_{reg} cell genes (Figures S6L–S6O). Neither did we find that MED1 protein expression was different in tumor T_{reg} cells relative to splenic T_{reg} cells (Figure S6P). This suggests that MED1 does not control expression of transcription factors involved in effector T_{reg} cell function, but rather controls their transcriptional activity. Therefore, MED1 seems to regulate

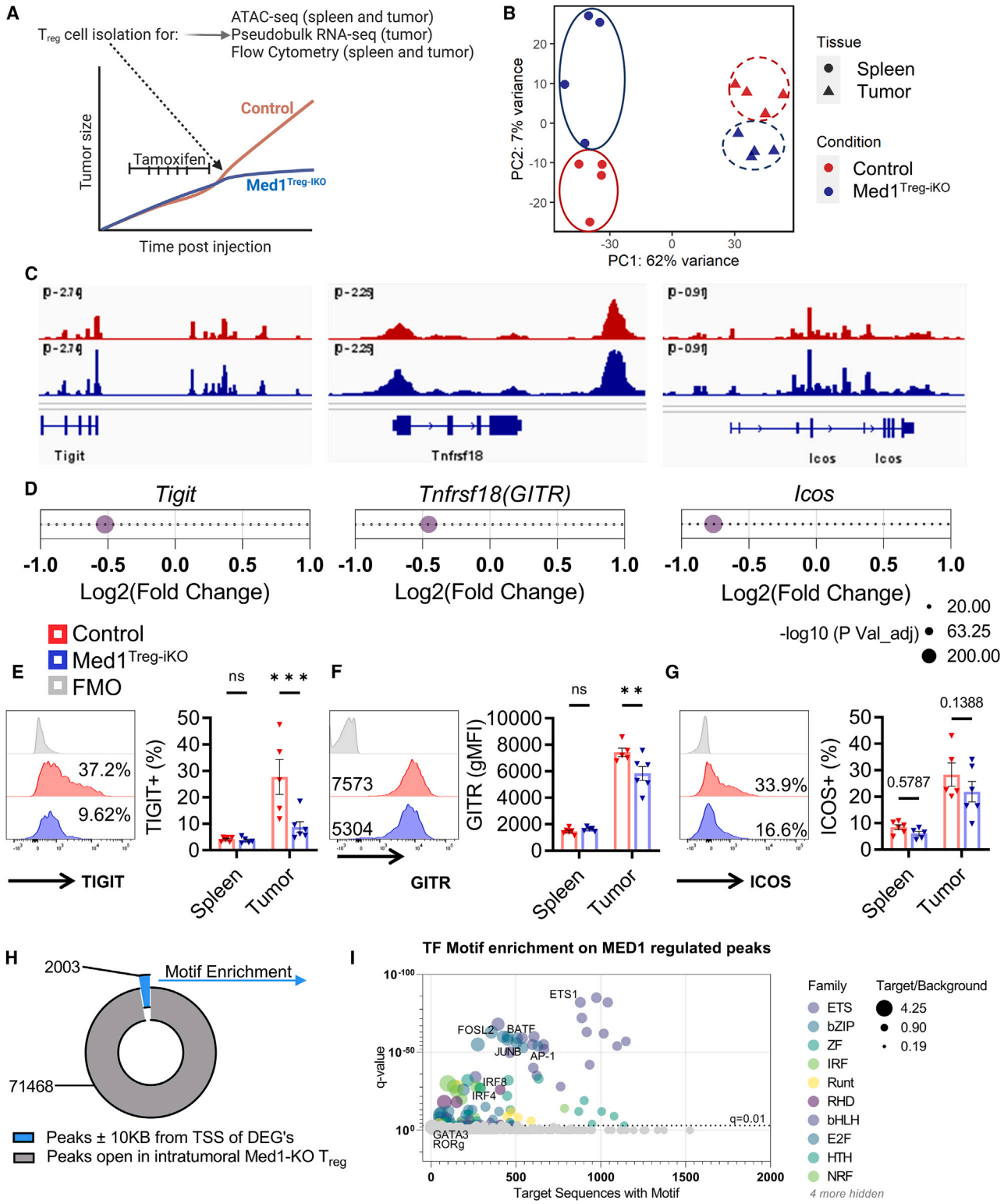

Figure 4. MED1 promotes transcription of T_{reg} cell terminal differentiation program independent of chromatin accessibility

(A) Experimental schematic of ATAC-sequencing and pseudobulk RNA sequencing experiments.

(B) Principal component analysis plot of ATAC-sequencing peaks based on Deseq2 output.

(C) ATAC-sequencing tracks of effector T_{reg} cell genes.

(legend continued on next page)

effector T_{reg} cell functions largely through gene transcription, independent of modulating chromatin accessibility.

Because we observed minimal differences in chromatin accessibility, we hypothesized that MED1 may act as co-activator for transcription factors to drive expression of effector genes. To infer these transcription factors, we filtered the accessible regions in intratumoral T_{reg} cells down to those 10 KB upstream or downstream of the transcription start sites of genes significantly downregulated due to MED1-deletion. Of the 71,468 accessible peaks, 2,003 were in regions associated with MED1 regulation (Figure 4H). We then used Hypergeometric Optimization of Motif EnRichment to find transcription factor motifs significantly enriched in this subset of peaks.[70] We found that the peaks were significantly enriched for the ETS (erythroblast transformation specific), basic leucine zipper, zinc finger, and IFN-regulatory factor (IRF) family of motifs (Figure 4I). Moreover we found that targets of transcription factors implicated in tumor T_{reg} cell differentiation, BATF, FOSL2, IRF4, and IRF8, were specifically enriched in the peak set (Figures 4I, S6D–S6G).[5,21,22] In contrast, while MED1 is known to be a co-activator for nuclear receptors (NRs) in other cell types, we found no enrichment for the NR family of motifs indicating that MED1 plays a cell type-specific role in T_{reg} cells distinct from its function in other contexts.[29,71,72] Consistent with our discovery of unaltered proportion of Th2-like T_{reg} cells, we did not find significant enrichment of motifs for GATA3 or RORγ, suggesting that MED1 is dispensable for the generation of Th2-like T_{reg} cells.

Collectively, these data demonstrate that, although MED1 is dispensable for modulating chromatin accessibility of T_{reg} cells, it is essential for enforcing transcription of specific effector T_{reg} cell transcription factors within tumors.

Murine and human T_{reg} cells experience divergent paths of differentiation in tumors relative to inflammation

Through our use of syngeneic tumor models and various *in vivo* models of inflammation, we infer that MED1 promotes tumor-specific functions of T_{reg} cells. We must acknowledge, however, that these models all occur in different tissues and begin with different stimuli, including T cell transfer, immunization, and infection. To further characterize MED1's role in promotion of T_{reg} cell suppression of antitumor immunity, we used two models that induce inflammation using the same chemical stimuli and occur in the same tissue. We first used a spontaneous model of cancer that uses a combination of azoxymethane and dextran sodium sulfate (DSS) to induce colitis-associated cancer (CAC).[73] In this model, the administration of chemical carcinogen is followed by repeated cycles of DSS to form tumors, recapitulating human CAC development (Figure 5A). After 12 weeks, we observed decreased tumor burden, decreased tumor number per colon, decreased individual tumor size, and a small increase in colon length in $Med1^{Treg-KO}$ mice (Figures 5B–5F). $Med1^{Treg-KO}$ mice did not show a difference in the severity of clinical colitis symptoms as measured by the disease activity index, but did show a statistically insignificant trend toward increased survival, likely due to reduced tumor burden (Figures 5G and 5H). Although we did not observe an increased severity of colitis, we wondered whether a mild increase in colitis-associated inflammation may be driving the reduced tumor growth in $Med1^{Treg-KO}$ mice. To assess this possibility, we compared control and $Med1^{Treg-KO}$ mice in a DSS model of acute colitis (Figure 5I). Importantly, we found no significant difference in the disease activity index, colon length, body weight decrease, histological evidence of inflammation, number of infiltrating T cells, or production of inflammatory cytokines (Figures 5J–5O, S7A–S7E). Moreover, we did not see significant differences in tumor effector T_{reg} cell molecules TIGIT or ICOS expression, despite a small decrease in GITR expression (Figures S7F–S7H). Nevertheless, the tumor effector program does not seem to be elicited in colonic inflammation to the same extent as in syngeneic tumor models (Figure S7F–S7H, 5E–5G). Last, we did not see significant differences in central T_{reg} cell populations in DSS colitis (Figure S7I). Collectively, these data suggests that the T_{reg} cells required for promoting tumor formation and growth in colons are distinct from those controlling colitis associated inflammation.

To dissect the divergent functional programs, we compared wildtype T_{reg} cells isolated from colons of mice with DSS-induced colitis with T_{reg} cells from colon-associated tumors in mice with CAC (Figure 6A). Integrated analysis of single cell RNA-sequencing data from 10,692 total T_{reg} cells revealed 8 distinct clusters of cells (Figure 6B). T_{reg} cells from tumors exhibited major overlap with those from inflamed colons indicating a considerable portion of T_{reg} cell phenotype is dictated by inflammatory status and anatomic location (Figures 6C, 6D, and S8A). Noticeably, T_{reg} cells isolated from tumors were overrepresented represented in cluster 5. Importantly, cluster 5 was marked by expression of *Ccr8*, *Tnfrsf18*, *Tnfrsf4*, and *Tnfrsf9. Ikzf2*, *Klrg1*, and, overall, a tumor-specific signature similar to that in clusters 4 and 5 from syngeneic tumor models, which frequency or suppressive gene expression are reduced by MED1 deletion (Figures 3E, 6E, and S8A). We then confirmed this signature (*Lag3*, *Tigit*, *Tnfrsf18*(*GITR*), *Tnfrsf4* (*OX40*), *Icos*, *Havcr2*

(D) Gene expression of effector T_{reg} cell genes MED1-deficient intratumoral T_{reg} cells relative to MED1-sufficient intratumoral T_{reg} cells from pseudobulk RNA sequencing using MAST package.
(E) Representative flow plots of TIGIT expression in intratumoral T_{reg} cells and summary data of splenic and intratumoral T_{reg} cells (n = 5 from controls and n = 6 $Med1^{Treg-IKO}$).
(F) Representative flow plots of GITR expression in intratumoral T_{reg} cells and summary data of splenic and intratumoral T_{reg} cells (n = 5 from controls and n = 6 $Med1^{Treg-IKO}$).
(G) Representative flow plots of ICOS expressions in intratumoral T_{reg} cells and summary data of splenic and intratumoral T_{reg} cells (n = 5 from control and n = 6 $Med1^{Treg-IKO}$).
(H) Quantification of ATAC-sequencing peaks ±10 KB from transcription start sites of significantly downregulated genes in MED1-deficient intratumoral T_{reg} cells.
(I) Transcription factor motif analysis on peaks from (H). Performed in Hypergeometric Optimization of Motif EnRichment. Gene expression differences were calculated with the MAST package. (E–G) used two-way ANOVA with multiple comparisons. I used HOMER to calculate motif enrichment, q-values are reported. (**$p < 0.01$, ****$p < 0.0001$.) Related to Figure S6.

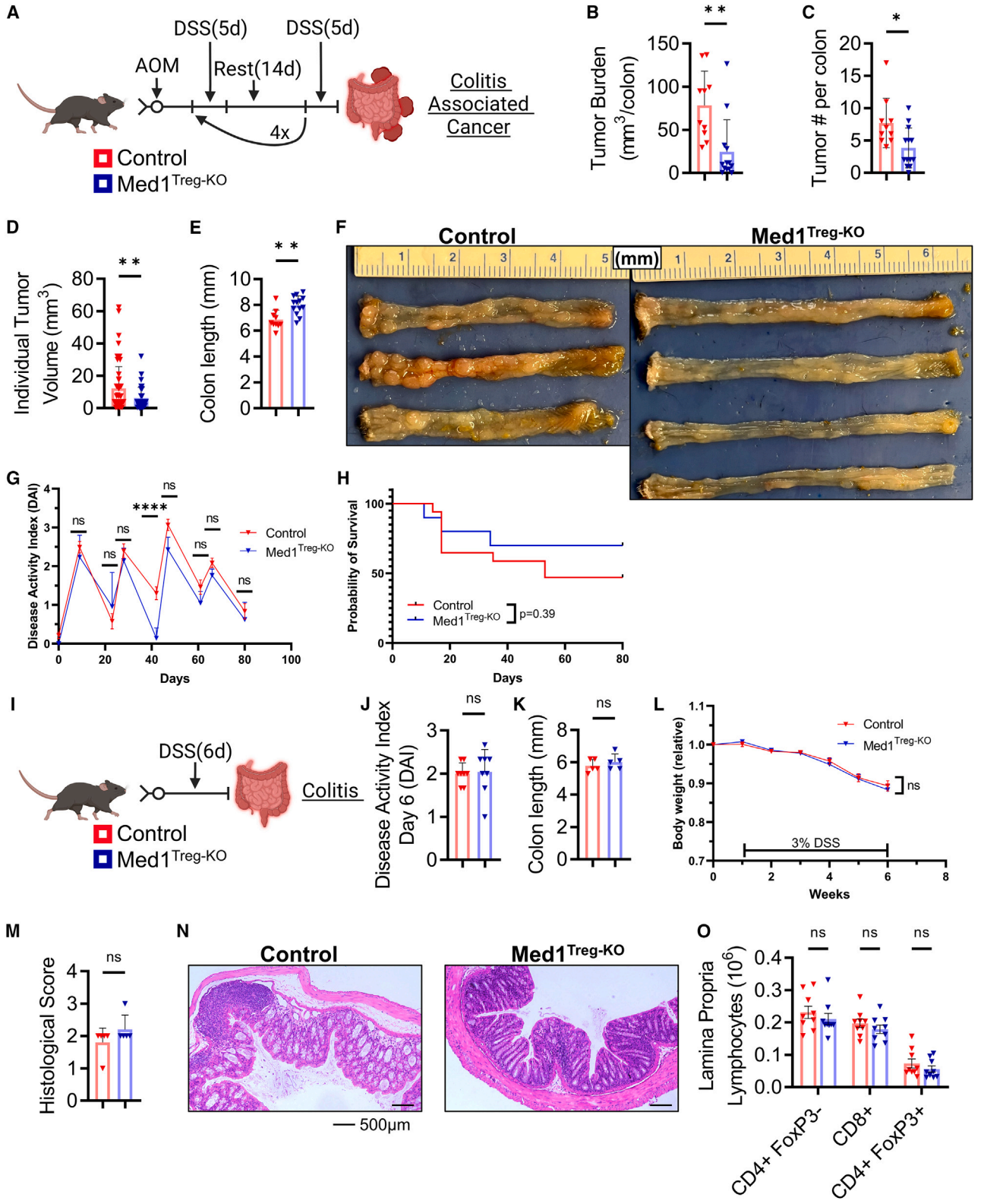

Figure 5. MED1 is required for T_{reg} cell promotion of colon tumor growth, but dispensable for control of colonic inflammation

(A) Experimental setup for colitis-associated-cancer model induced by azoxymethane (AOM)/dextran sodium sulfate (DSS) treatment.

(B) Tumor burden per colon (n = 10 controls and n = 13 $Med1^{Treg-KO}$).

(legend continued on next page)

(*TIM-3*), and *Ccr8*) was elevated specifically in cluster 5 through module scoring (Figure 6F). Noticeably, *Batf* and *Irf4* expression were not restricted to cluster 5, supporting the notion that these transcription factors program general effector T_{reg} cell function in tissues, rather than only in tumors (Figure S8E).

Similar to our single-cell RNA sequencing data of T_{reg} cells in syngeneic tumors, we identified a central-like T_{reg} cell population (cluster 1) with relatively higher expression of *Klf2*, *Tcf7*, *Ccr7*, and *S1pr1* in both colitis and CAC (Figures S8A and S8B). In addition, we identified a distinct cluster marked by expression of *Maf*,[75] *Il17a*, *Il10*, *Ctla4*, and *Lag3*. likely representing an effector Th17-like T_{reg} cell population (cluster 2) (Figures S8A and S8C).[76] While cluster 2 was more prevalent in tumors it still comprised a relatively high proportion (20%) of T_{reg} cells identified in acute colitis (Figure 6D).

To gain insight into the transcriptional orchestrators of the divergence of the cluster 2 and cluster 5 effector T_{reg} cells, we performed a differential expression analysis and identified transcription factors *Ikzf2*, *Bmyc*, *Rel*, *Nr4a1*, and *Nr4a2* associated with cluster 5, whereas *Maf* and *Ikzf3* associated with cluster 2 (Figure S8F). To infer key mediators of this differentiation path, we performed a trajectory analysis and used the graph test function in Monocle3 (Figure 6G). The graph test computes Moran's I for all genes expressed, determining spatial autocorrelation, which indicates whether a gene is associated with pseudotime with statistical significance. From this analysis, we identified *Jun* and *Fos* (AP-1 family members) and *Ikzf2* (HELIOS) as key mediators of the differentiation path, leading to tumor-specific T_{reg} cells in cluster 5 (Figure 6H). These transcription factor's binding motifs were also enriched in intratumoral MED1 regulated peaks suggesting MED1 may enable differentiation along this path in concert with JUN, FOS, and IKZF2 (Figures 4I and 6H).

Finally, we sought to confirm whether our findings in mice were consistent with human disease. We used a previously published dataset[77] that compared intratumoral T cells in patients with head and neck squamous cell carcinoma (HNSCC) with T cells from non-malignant, inflamed tissue in the oral mucosa (OM) (Figure 6I). We isolated the T_{reg} cells from the dataset based on positive *CD4*, *FOXP3*, and *IL2RA* expression and negative *IL2* expression (Figure S8H) and performed an integrated analysis to compare human T_{reg} cell tissue heterogeneity to our mouse data (Figure S8I). Importantly, this analysis identified a cluster of T_{reg} cells, displaying a tumor-specific suppression signature (cluster 5, *TIGIT BATF*, *TNFRSF4*, and *TNFRSF18*), were enriched in HNSCC relative to inflamed OM tissues similar to our findings in mice (Figures 6J–6L).

Collectively, these data suggest, independent of tissue type and inflammation, that tumors promote the development of a specialized effector T_{reg} cell subset.

DISCUSSION

The importance of T_{reg} cells in maintaining immune system homeostasis juxtaposed against their role in promoting tumor growth has posed challenges to targeting T_{reg} cells for cancer therapies. Given the indispensable role of T_{reg} cells in preventing autoimmunity, suppression of T_{reg} cells is anticipated to elicit autoimmune inflammatory responses. Indeed, checkpoint blockade immune therapy can cause fatal autoimmune inflammatory effects in patients with cancer.[9] Our study identifies tumor-intrinsic T_{reg} cell differentiation as a therapeutic niche for eliciting antitumor immunity without triggering autoimmune consequences. We present a study of the Mediator complex in T_{reg} cells and find that MED1 is dispensable for maintaining FOXP3 expression and immune system homeostasis in adult mice. Surprisingly, suppression of MED1 in T_{reg} cells antagonized tumor growth and enhanced $CD8^+$ T cell infiltration and function.

We discovered that MED1 drives a tumor-specific T_{reg} differentiation program crucial for suppressing $CD8^+$ T cell antitumor immunity. Through our study, we identified highly differentiated populations of tumor T_{reg} cells that displayed enhanced expression of suppressive molecules such as *Tigit*, *Tnfrsf18*, *Tnfrsf9*, *Icos*, and *Ccr8*. Similarly, others have shown that this $ICOS^{hi}$, $CCR8^+$ T_{reg} cell subset exhibits superior suppressive capacity when compared with other T_{reg} cells.[22,61,62] MED1-deficient T_{reg} cells were able to traffic to tumors and establish multiple functional T_{reg} cell subsets, but failed to generate adequate tumor immunity suppressing T_{reg} cell subsets. Previous studies have focused on the differentiation of T_{reg} cells from lymphoid organs, to blood, to tumor, suggesting that T_{reg} cells may arrive at tumors fully differentiated.[21,23] Our data support the model[78] that posits that T_{reg} cells get primed in lymphoid tissues, but experience their final diversification at the tissue site. Further work could explore how different populations of T_{reg} cells enter, respond to specific antigens, localize, and traffic out of tumor

(C) Tumor number per colon (n = 10 controls and n = 13 $Med1^{Treg-KO}$).
(D) Individual tumor volume (n = 10 controls and n = 13 $Med1^{Treg-KO}$). Points represent individual tumors.
(E) Colon length (n = 10 controls and n = 13 $Med1^{Treg-KO}$).
(F) Representative photographs of opened colons from control and $Med1^{Treg-KO}$ mice.
(G) Disease activity index measured weekly. (n = 10 controls and n = 13 $Med1^{Treg-KO}$.)
(H) Survival of mice during duration of experiment.
(I) Experimental setup for DSS treatment for colitis induction.
(J) Disease activity index measured at experiment conclusion (n = 8 controls and n = 8 $Med1^{Treg-KO}$).
(K) Colon length (n = 5 controls and n = 5 $Med1^{Treg-KO}$).
(L) Bodyweight relative to start (n = 8 controls and n = 8 $Med1^{Treg-KO}$).
(M) Summary of histological score (n = 5 controls and n = 5 $Med1^{Treg-KO}$).
(N) Representative hematoxylin and eosin staining from the colons of mice.
(O) Quantification of infiltrating lamina propria lymphocytes (n = 9 controls and n = 9 $Med1^{Treg-KO}$). (B–E), (J), (K), and (M) use unpaired Student's two-tailed t test at experiment conclusion. (G), (L), and (O) used two-way ANOVA with multiple comparisons. Bars represent ± SEM. Points on graph except for (D) represent individual mice. (*$p < 0.05$, **$p < 0.01$, ****$p < 0.0001$.) Related to Figure S7.

CellPress
OPEN ACCESS

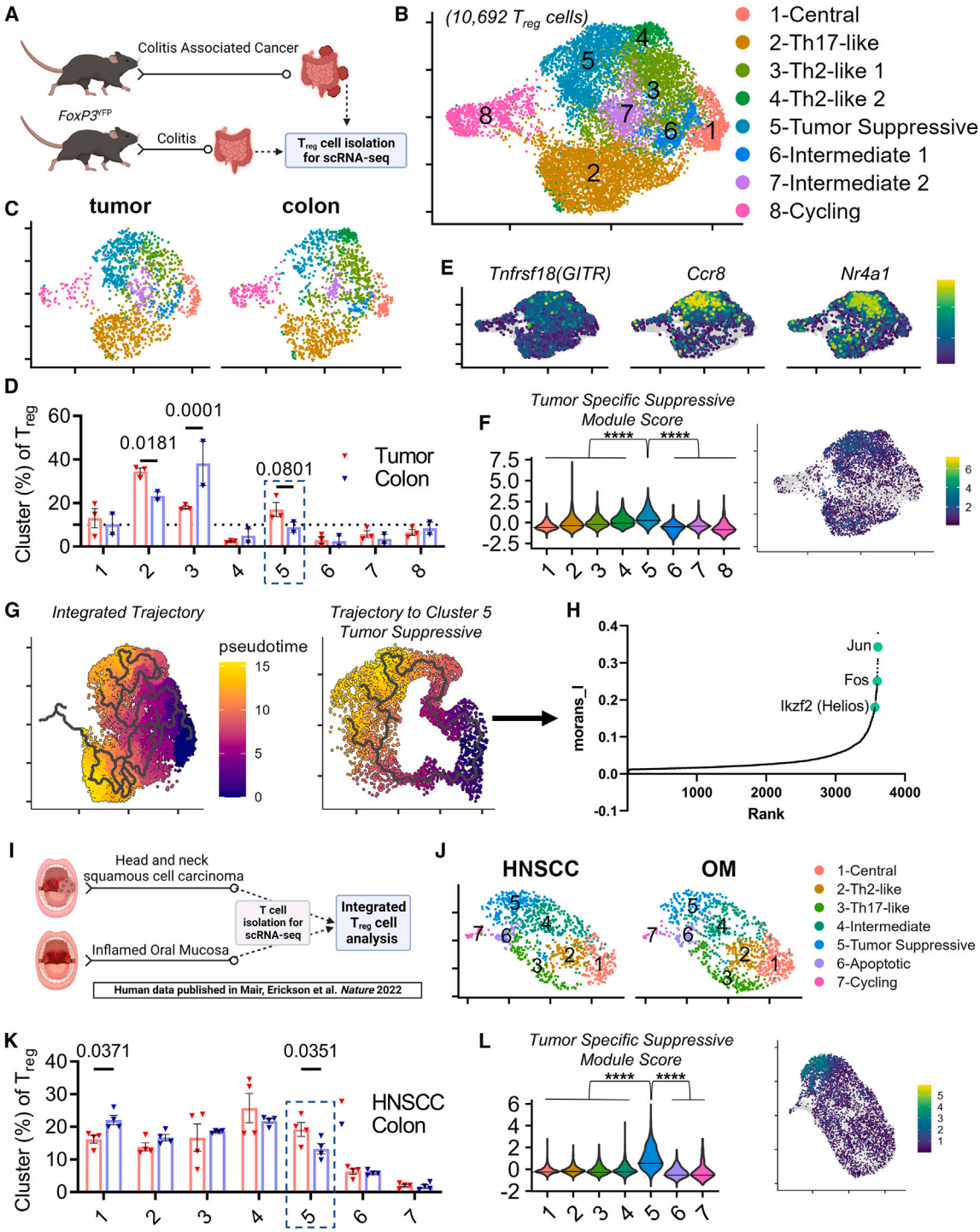

Figure 6. Murine and human T_{reg} cells experience divergent paths of differentiation in tumors relative to inflammation

(A) Experimental setup for colitis-associated-cancer model and colitis experiments.

(B) Integrated UMAP clustering of T_{reg} cells isolated from tumors and colons.

(C) UMAP diagrams of T_{reg} cells isolated from tumors and colons.

(D) Cluster proportion of total T_{reg} cells from different conditions (n = 2–3 biological replicates per condition, each biological replicate contains cells pooled from 2 to 8 separate mice). p values of less than 0.1 are displayed.

(E) Feature plots of cluster 5 enriched genes.

(F) Tumor-specific suppressive module score violin plot and UMAP plot.

(legend continued on next page)

sites, which may explain differences we saw in intratumoral T_{reg} cells in our study. Indeed, other groups have used single cell T cell receptor sequencing to demonstrate highly suppressive T_{reg} cell populations may be clonally expanded.[57,63]

At the molecular level, we have shown that MED1 is an essential factor for promoting the transcription of a tumor-suppressive T_{reg} cell program independent of the chromatin landscape. Our analysis has revealed MED1 likely acts as a co-activator for well described tissue-programming transcription factors, such as IRF4 and BATF,[21,22] and implicated factors such as AP-1 family members and IKZF2 as more specific determinants of tumor effector T_{reg} cell differentiation. Importantly, we show that MED1 does not regulate the expression of transcription factors, but rather the expression of a subset of their target genes. We could not dissect whether this stems from limited transcription factor recruitment to target sites or a limited ability to recruit polymerase II to target sites due to technical limitations stemming from limited amounts of intratumoral T_{reg} cells, where we focused our study. Based on prior studies of MED1 function in adipocyte expansion, however, we hypothesize this is due to impaired Mediator complex function and compromised ability to recruit RNA polymerase II.[33] Interestingly, this demonstrates that MED1 exercises divergent roles from other Mediator complex subunits, which CRISPR screens have identified as regulators of FOXP3 expression, unlike MED1.[37,74] Our CRISPR screen based on the changes in FOXP3 expression did not show an enrichment of MED1.[37] Consistently, our discovery here is that MED1 deletion does not alter FoxP3 levels. This highlights the complexity of the Mediator complex and the potential for differential confirmations of Mediator complexes to exercise distinct functions within T_{reg} cells.

Our study highlights the potential to identify precision immunotherapies by interrogating T_{reg} cells in similar but distinct settings. By analyzing T_{reg} cells from colons in colitis and tumors from colitis-associated cancer, we were able to identify divergent effector programs within the T_{reg} cell compartment. The MAF-controlled T_{reg} cell subset is associated with IL-10 production and essential for maintaining intestinal homeostasis, as previously described.[75,76,79] Depletion of this T_{reg} cell subset would likely lead to severe colitis if attempted in patients with colon cancer. Our analysis revealed a divergent T_{reg} cell subset consistent with the tumor-suppressive signature we previously described. Depletion of this subset, through suppression of MED1 or its activating pathways, could potentially aid in the treatment of colon cancer without compromising intestinal homeostasis, and CCR8 depletion of the tumor suppressive T_{reg} cell subset has indeed been used successfully in mouse models of MC38 colon adenocarcinoma.[63]

The targeting of tumor-specific T_{reg} cell differentiation represents a therapeutic strategy for cancer that alleviates the detrimental autoimmune consequences of current effective immunotherapies. MED1 represents a node in this pathway and highlights the opportunity to more completely dissect divergent T_{reg} cell functions based on situational and environmental context. One potential strategy for preventing tumor specific suppressor T_{reg} differentiation is through modulation of MED1 function. Phosphorylation of MED1 is known to regulate its ability to promote transcription, but it is unclear how phosphorylation of MED1 influences its activity in T_{reg} cells.[80] Cyclin-dependent kinase 7 (CDK7), which phosphorylates MED1, currently has inhibitors in clinical trials that may have dual chemotherapeutic and immunotherapeutic effects.[81–84] Dissecting the influence of CDK7 directly on MED1 in intratumoral T_{reg} cells is challenging, however, due to the promiscuous kinase activity of CDK7 and the robust tumor-intrinsic effect of the drug. Further study of T_{reg} cells through comparisons in different contexts may elucidate additional precision immunotherapeutic strategies with situational specificity.

Limitations of the study

Our study demonstrates that MED1 promotes T_{reg} cell function specifically in the tumor microenvironment in a $CD8^+$ T cell dependent manner. We did not provide data on whether this is occurring through other intermediate cell types, although recent work indicates myeloid and endothelial cells may be important downstream effectors of T_{reg} cells. We additionally were unable to discern what the specific molecule, ontological factor, or physiochemical factor making MED1 specific to tumor T_{reg} cell function, largely due to the limited T_{reg} cell number that can be obtained from tumors. Last, technical challenges precluded us from discerning MED1 genomic localization in tumor T_{reg} cells. MED1 is a factor that loosely binds chromatin, thus retaining its genomic localization requires fixation, which paradoxically makes techniques such as CUT&TAG lose the low-input advantage it normally provides.

STAR★METHODS

Detailed methods are provided in the online version of this paper and include the following:

- KEY RESOURCES TABLE
- RESOURCE AVAILABILITY
  - Lead contact
  - Materials availability
  - Data and code availability

(G) Pseudotime representation portrayed on integrated UMAP plot and specific trajectory toward cluster 5.
(H) Graph test results from Monocle 3. Moran's I plotted for genes from least to greatest. Transcription factors above 0.2 labeled.
(I) Experimental setup from (Loo et al.[74]). $CD3^+$ T cells were isolated from patients, then T_{reg} cells were subset during analysis based on positive *CD4*, *FOXP3*, and *IL2RA* expression and negative *IL2* expression.
(J) UMAP plots of T_{reg} cells from HNSCC and inflamed OM.
(K) Cluster proportion of total T_{reg} cells from different conditions (n = 4 biological replicates per condition). p values of less than 0.1 are displayed.
(L) Tumor-specific suppressive module score violin plot and UMAP plots for human data. (D) and (K) used two-way ANOVA with multiple comparisons. (F) and (L) used one-way ANOVA with Dunnet's multiple comparisons test to compare cluster 5 to all clusters. (I) uses the graph test (Moran's I) to test for genes with multi-directional and multi-dimensional spatial autocorrelation. Related to Figure S8.

SUPPLEMENTAL INFORMATION

Supplemental information can be found online at https://doi.org/10.1016/j.xcrm.2024.101441.

ACKNOWLEDGMENTS

We thank members of the Fang Laboratory for technical advice and discussion. We thank Dr. Jindan Yu and Dr. Bin Zhang for supplying tumor cell lines. This work was supported by the Northwestern University RHLCCC Flow Cytometry Facility and a Cancer Center Support Grant (NCI CA060553). Histology services were provided by the Northwestern University Mouse Histology and Phenotyping Laboratory, which is supported by (NCI P30-CA060553) awarded to the Robert H. Lurie Comprehensive Cancer Center. The single-cell library preparation and sequencing was done at Northwestern University NUseq facility core with the support of NIH Grant (1S10OD025120). S.M.C. was supported by T32DK007169. M.A.T. was supported by T32HL076139. B.D.S. was supported by R01HL149883, R01HL153122, P01HL154998, and U19AI135964. R.S. was supported by the Crohn's & Colitis Foundation Senior Research Award, R01DK124199, and RO1AI153568. D.F. was supported by R01CA257520, R01CA232347, R01DK126908, and R01DK120330.

AUTHOR CONTRIBUTIONS

Conceptualization: S.M.C., S.E.W., and D.F.; methodology, S.M.C., Y.Z., S.E.W., and D.F.; investigation, S.M.C., Y.Z, E.M., L.Y., R.I., A.T., M,A,T., N.M., S.W., K.L., W.L., T.M.B., Z.D., L.M., C.W., B.G., J.W., R.S., and S.E.W.; formal analysis, S.M.C., Y.Z., D.W., and J.S.; writing – original draft, S.M.C; writing – review & and editing, S.M.C., S.E.W., and D.F.; funding acquisition, F.Y., W.C., B.D.S., R.S., and D.F.; supervision, D.F.

DECLARATION OF INTERESTS

B.D.S. holds United States Patent No. US 10,905,706 B2, "Compositions and Methods to Accelerate Resolution of Acute Lung Inflammation" and serves on the Scientific Advisory Board of Zoe Biosciences, outside of the submitted work.

Received: August 9, 2023
Revised: December 18, 2023
Accepted: February 1, 2024
Published: February 29, 2024

REFERENCES

1. Khattri, R., Cox, T., Yasayko, S.-A., and Ramsdell, F. (2003). An essential role for Scurfin in CD4+CD25+ T regulatory cells. Nat. Immunol. *4*, 337–342. https://doi.org/10.1038/ni909.
2. Hori, S., Nomura, T., and Sakaguchi, S. (2003). Control of regulatory T cell development by the transcription factor Foxp3. Science *299*, 1057–1061. https://doi.org/10.1126/science.1079490.
3. Fontenot, J.D., Gavin, M.A., and Rudensky, A.Y. (2003). Foxp3 programs the development and function of CD4+CD25+ regulatory T cells. Nat. Immunol. *4*, 330–336. https://doi.org/10.1038/ni904.
4. Salama, P., Phillips, M., Grieu, F., Morris, M., Zeps, N., Joseph, D., Platell, C., and Iacopetta, B. (2009). Tumor-infiltrating FOXP3+ T regulatory cells show strong prognostic significance in colorectal cancer. J. Clin. Oncol. *27*, 186–192. https://doi.org/10.1200/JCO.2008.18.7229.
5. Plitas, G., Konopacki, C., Wu, K., Bos, P.D., Morrow, M., Putintseva, E.V., Chudakov, D.M., and Rudensky, A.Y. (2016). Regulatory T cells exhibit distinct features in human breast cancer. Immunity *45*, 1122–1134. https://doi.org/10.1016/j.immuni.2016.10.032.
6. Karpisheh, V., Mousavi, S.M., Naghavi Sheykholeslami, P., Fathi, M., Mohammadpour Saray, M., Aghebati-Maleki, L., Jafari, R., Majidi Zolbanin, N., and Jadidi-Niaragh, F. (2021). The role of regulatory T cells in the pathogenesis and treatment of prostate cancer. Life Sci. *284*, 119132. https://doi.org/10.1016/j.lfs.2021.119132.
7. Curiel, T.J., Coukos, G., Zou, L., Alvarez, X., Cheng, P., Mottram, P., Evdemon-Hogan, M., Conejo-Garcia, J.R., Zhang, L., Burow, M., et al. (2004). Specific recruitment of regulatory T cells in ovarian carcinoma fosters immune privilege and predicts reduced survival. Nat. Med. *10*, 942–949. https://doi.org/10.1038/nm1093.
8. Sato, E., Olson, S.H., Ahn, J., Bundy, B., Nishikawa, H., Qian, F., Jungbluth, A.A., Frosina, D., Gnjatic, S., Ambrosone, C., et al. (2005). Intraepithelial CD8+ tumor-infiltrating lymphocytes and a high CD8+/regulatory T cell ratio are associated with favorable prognosis in ovarian cancer. Proc. Natl. Acad. Sci. USA *102*, 18538–18543. https://doi.org/10.1073/pnas.0509182102.
9. Sawant, D.V., Yano, H., Chikina, M., Zhang, Q., Liao, M., Liu, C., Callahan, D.J., Sun, Z., Sun, T., Tabib, T., et al. (2019). Adaptive plasticity of IL-10 + and IL-35 + T reg cells cooperatively promotes tumor T cell exhaustion. Nat. Immunol. *20*, 724–735. https://doi.org/10.1038/s41590-019-0346-9.
10. Collison, L.W., Workman, C.J., Kuo, T.T., Boyd, K., Wang, Y., Vignali, K.M., Cross, R., Sehy, D., Blumberg, R.S., and Vignali, D.A.A. (2007). The inhibitory cytokine IL-35 contributes to regulatory T-cell function. Nature *450*, 566–569. https://doi.org/10.1038/nature06306.
11. Deaglio, S., Dwyer, K.M., Gao, W., Friedman, D., Usheva, A., Erat, A., Chen, J.-F., Enjyoji, K., Linden, J., Oukka, M., et al. (2007). Adenosine generation catalyzed by CD39 and CD73 expressed on regulatory T cells mediates immune suppression. J. Exp. Med. *204*, 1257–1265. https://doi.org/10.1084/jem.20062512.
12. Zappasodi, R., Serganova, I., Cohen, I.J., Maeda, M., Shindo, M., Senbabaoglu, Y., Watson, M.J., Leftin, A., Maniyar, R., Verma, S., et al. (2021). CTLA-4 blockade drives loss of Treg stability in glycolysis-low tumours. Nature *591*, 652–658. https://doi.org/10.1038/s41586-021-03326-4.
13. Tan, C.L., Kuchroo, J.R., Sage, P.T., Liang, D., Francisco, L.M., Buck, J., Thaker, Y.R., Zhang, Q., McArdel, S.L., Juneja, V.R., et al. (2021). PD-1 restraint of regulatory T cell suppressive activity is critical for immune tolerance. J. Exp. Med. *218*, e20182232. https://doi.org/10.1084/jem.20182232.
14. Arpaia, N., Green, J.A., Moltedo, B., Arvey, A., Hemmers, S., Yuan, S., Treuting, P.M., and Rudensky, A.Y. (2015). A Distinct Function of

Regulatory T Cells in Tissue Protection. Cell *162*, 1078–1089. https://doi.org/10.1016/j.cell.2015.08.021.

15. Delgoffe, G.M., Woo, S.-R., Turnis, M.E., Gravano, D.M., Guy, C., Overacre, A.E., Bettini, M.L., Vogel, P., Finkelstein, D., Bonnevier, J., et al. (2013). Regulatory T cell stability is maintained by a neuropilin-1:semaphorin-4a axis. Nature *501*, 252–256. https://doi.org/10.1038/nature12428.
16. Onda, M., Kobayashi, K., and Pastan, I. (2019). Depletion of regulatory T cells in tumors with an anti-CD25 immunotoxin induces CD8 T cell-mediated systemic antitumor immunity. Proc. Natl. Acad. Sci. USA *116*, 4575–4582. https://doi.org/10.1073/pnas.1820388116.
17. Delaunay, M., Prévot, G., Collot, S., Guilleminault, L., Didier, A., and Mazières, J. (2019). Management of pulmonary toxicity associated with immune checkpoint inhibitors. Eur. Respir. Rev. *28*, 190012. https://doi.org/10.1183/16000617.0012-2019.
18. Conroy, M., and Naidoo, J. (2022). Immune-related adverse events and the balancing act of immunotherapy. Nat. Commun. *13*, 392. https://doi.org/10.1038/s41467-022-27960-2.
19. Suresh, K., and Naidoo, J. (2020). Lower Survival in Patients Who Develop Pneumonitis Following Immunotherapy for Lung Cancer. Clin. Lung Cancer *21*, e169–e170. https://doi.org/10.1016/j.cllc.2019.10.009.
20. Kamada, T., Togashi, Y., Tay, C., Ha, D., Sasaki, A., Nakamura, Y., Sato, E., Fukuoka, S., Tada, Y., Tanaka, A., et al. (2019). PD-1+ regulatory T cells amplified by PD-1 blockade promote hyperprogression of cancer. Proc. Natl. Acad. Sci. USA *116*, 9999–10008. https://doi.org/10.1073/pnas.1822001116.
21. Itahashi, K., Irie, T., Yuda, J., Kumagai, S., Tanegashima, T., Lin, Y.-T., Watanabe, S., Goto, Y., Suzuki, J., Aokage, K., et al. (2022). BATF epigenetically and transcriptionally controls the activation program of regulatory T cells in human tumors. Sci. Immunol. *7*, eabk0957. https://doi.org/10.1126/sciimmunol.abk0957.
22. Alvisi, G., Brummelman, J., Puccio, S., Mazza, E.M., Tomada, E.P., Losurdo, A., Zanon, V., Peano, C., Colombo, F.S., Scarpa, A., et al. (2020). IRF4 instructs effector Treg differentiation and immune suppression in human cancer. J. Clin. Invest. *130*, 3137–3150. https://doi.org/10.1172/JCI130426.
23. Miragaia, R.J., Gomes, T., Chomka, A., Jardine, L., Riedel, A., Hegazy, A.N., Whibley, N., Tucci, A., Chen, X., Lindeman, I., et al. (2019). Single-Cell Transcriptomics of Regulatory T Cells Reveals Trajectories of Tissue Adaptation. Immunity *50*, 493–504.e7. https://doi.org/10.1016/j.immuni.2019.01.001.
24. Cipolletta, D., Feuerer, M., Li, A., Kamei, N., Lee, J., Shoelson, S.E., Benoist, C., and Mathis, D. (2012). PPAR-γ is a major driver of the accumulation and phenotype of adipose tissue Treg cells. Nature *486*, 549–553. https://doi.org/10.1038/nature11132.
25. DiSpirito, J.R., Zemmour, D., Ramanan, D., Cho, J., Zilionis, R., Klein, A.M., Benoist, C., and Mathis, D. (2018). Molecular diversification of regulatory T cells in nonlymphoid tissues. Sci. Immunol. *3*, eaat5861. https://doi.org/10.1126/sciimmunol.aat5861.
26. Hayatsu, N., Miyao, T., Tachibana, M., Murakami, R., Kimura, A., Kato, T., Kawakami, E., Endo, T.A., Setoguchi, R., Watarai, H., et al. (2017). Analyses of a Mutant Foxp3 Allele Reveal BATF as a Critical Transcription Factor in the Differentiation and Accumulation of Tissue Regulatory T Cells. Immunity *47*, 268–283.e9. https://doi.org/10.1016/j.immuni.2017.07.008.
27. Magnuson, A.M., Kiner, E., Ergun, A., Park, J.S., Asinovski, N., Ortiz-Lopez, A., Kilcoyne, A., Paoluzzi-Tomada, E., Weissleder, R., Mathis, D., and Benoist, C. (2018). Identification and validation of a tumor-infiltrating Treg transcriptional signature conserved across species and tumor types. Proc. Natl. Acad. Sci. USA *115*, E10672–E10681. https://doi.org/10.1073/pnas.1810580115.
28. Chen, W., and Roeder, R.G. (2007). The Mediator subunit MED1/TRAP220 is required for optimal glucocorticoid receptor-mediated transcription activation. Nucleic Acids Res. *35*, 6161–6169. https://doi.org/10.1093/nar/gkm661.
29. Jia, Y., Viswakarma, N., and Reddy, J.K. (2014). Med1 Subunit of the Mediator Complex in Nuclear Receptor-Regulated Energy Metabolism, Liver Regeneration, and Hepatocarcinogenesis. Gene Expr. *16*, 63–75. https://doi.org/10.3727/105221614X13919976902219.
30. Chen, W., Zhang, X., Birsoy, K., and Roeder, R.G. (2010). A muscle-specific knockout implicates nuclear receptor coactivator MED1 in the regulation of glucose and energy metabolism. Proc. Natl. Acad. Sci. USA *107*, 10196–10201. https://doi.org/10.1073/pnas.1005626107.
31. Allen, B.L., and Taatjes, D.J. (2015). The Mediator complex: a central integrator of transcription. Nat. Rev. Mol. Cell Biol. *16*, 155–166. https://doi.org/10.1038/nrm3951.
32. Soutourina, J. (2018). Transcription regulation by the Mediator complex. Nat. Rev. Mol. Cell Biol. *19*, 262–274. https://doi.org/10.1038/nrm.2017.115.
33. Jang, Y., Park, Y.-K., Lee, J.-E., Wan, D., Tran, N., Gavrilova, O., and Ge, K. (2021). MED1 is a lipogenesis coactivator required for postnatal adipose expansion. Genes Dev. *35*, 713–728. https://doi.org/10.1101/gad.347583.120.
34. Yue, X., Izcue, A., and Borggrefe, T. (2011). Essential role of Mediator subunit Med1 in invariant natural killer T-cell development. Proc. Natl. Acad. Sci. USA *108*, 17105–17110. https://doi.org/10.1073/pnas.1109095108.
35. Jiang, P., Hu, Q., Ito, M., Meyer, S., Waltz, S., Khan, S., Roeder, R.G., and Zhang, X. (2010). Key roles for MED1 LxxLL motifs in pubertal mammary gland development and luminal-cell differentiation. Proc. Natl. Acad. Sci. USA *107*, 6765–6770. https://doi.org/10.1073/pnas.1001814107.
36. Montauti, E., Weinberg, S.E., Chu, P., Chaudhuri, S., Mani, N.L., Iyer, R., Zhou, Y., Zhang, Y., Liu, C., Xin, C., et al. (2022). A deubiquitination module essential for Treg fitness in the tumor microenvironment. Sci. Adv. *8*, eabo4116. https://doi.org/10.1126/sciadv.abo4116.
37. Cortez, J.T., Montauti, E., Shifrut, E., Gatchalian, J., Zhang, Y., Shaked, O., Xu, Y., Roth, T.L., Simeonov, D.R., Zhang, Y., et al. (2020). CRISPR Screen in Regulatory T Cells Reveals Novel Modulators of FoxP3. Nature *582*, 416–420.
38. El Khattabi, L., Zhao, H., Kalchschmidt, J., Young, N., Jung, S., Van Blerkom, P., Kieffer-Kwon, P., Kieffer-Kwon, K.-R., Park, S., Wang, X., et al. (2019). A Pliable Mediator Acts as a Functional Rather Than an Architectural Bridge between Promoters and Enhancers. Cell *178*, 1145–1158.e20. https://doi.org/10.1016/j.cell.2019.07.011.
39. Jia, Y., Qi, C., Kashireddi, P., Surapureddi, S., Zhu, Y.-J., Rao, M.S., Le Roith, D., Chambon, P., Gonzalez, F.J., and Reddy, J.K. (2004). Transcription Coactivator PBP, the Peroxisome Proliferator-activated Receptor (PPAR)-binding Protein, Is Required for PPARα-regulated Gene Expression in Liver. J. Biol. Chem. *279*, 24427–24434. https://doi.org/10.1074/jbc.M402391200.
40. Smigiel, K.S., Richards, E., Srivastava, S., Thomas, K.R., Dudda, J.C., Klonowski, K.D., and Campbell, D.J. (2014). CCR7 provides localized access to IL-2 and defines homeostatically distinct regulatory T cell subsets. J. Exp. Med. *211*, 121–136. https://doi.org/10.1084/jem.20131142.
41. Franckaert, D., Dooley, J., Roos, E., Floess, S., Huehn, J., Luche, H., Fehling, H.J., Liston, A., Linterman, M.A., and Schlenner, S.M. (2015). Promiscuous Foxp3-cre activity reveals a differential requirement for CD28 in Foxp3^{+} and Foxp3^{-} T cells. Immunol. Cell Biol. *93*, 417–423. https://doi.org/10.1038/icb.2014.108.
42. Collison, L.W., and Vignali, D.A.A. (2011). In Vitro Treg Suppression Assays. Methods Mol. Biol. *707*, 21–37. https://doi.org/10.1007/978-1-61737-979-6_2.
43. Rubtsov, Y.P., Rasmussen, J.P., Chi, E.Y., Fontenot, J., Castelli, L., Ye, X., Treuting, P., Siewe, L., Roers, A., Henderson, W.R., et al. (2008). Regulatory T Cell-Derived Interleukin-10 Limits Inflammation at Environmental Interfaces. Immunity *28*, 546–558. https://doi.org/10.1016/j.immuni.2008.02.017.

44. Chaudhary, B., and Elkord, E. (2016). Regulatory T Cells in the Tumor Microenvironment and Cancer Progression: Role and Therapeutic Targeting. Vaccines (Basel) *4*. https://doi.org/10.3390/vaccines4030028.

45. Togashi, Y., Shitara, K., and Nishikawa, H. (2019). Regulatory T cells in cancer immunosuppression — implications for anticancer therapy. Nat. Rev. Clin. Oncol. *16*, 356–371. https://doi.org/10.1038/s41571-019-0175-7.

46. Tosolini, M., Kirilovsky, A., Mlecnik, B., Fredriksen, T., Mauger, S., Bindea, G., Berger, A., Bruneval, P., Fridman, W.-H., Pagès, F., and Galon, J. (2011). Clinical impact of different classes of infiltrating T cytotoxic and helper cells (Th1, th2, treg, th17) in patients with colorectal cancer. Cancer Res. *71*, 1263–1271. https://doi.org/10.1158/0008-5472.CAN-10-2907.

47. Guo, Z., Wang, G., Wu, B., Chou, W.-C., Cheng, L., Zhou, C., Lou, J., Wu, D., Su, L., Zheng, J., et al. (2020). DCAF1 regulates Treg senescence via the ROS axis during immunological aging. J. Clin. Invest. *130*, 5893–5908. https://doi.org/10.1172/JCI136466.

48. Yamada, A., Arakaki, R., Saito, M., Tsunematsu, T., Kudo, Y., and Ishimaru, N. (2016). Role of regulatory T cell in the pathogenesis of inflammatory bowel disease. World J. Gastroenterol. *22*, 2195–2205. https://doi.org/10.3748/wjg.v22.i7.2195.

49. Koutrolos, M., Berer, K., Kawakami, N., Wekerle, H., and Krishnamoorthy, G. (2014). Treg cells mediate recovery from EAE by controlling effector T cell proliferation and motility in the CNS. Acta Neuropathol. Commun. *2*, 163. https://doi.org/10.1186/s40478-014-0163-1.

50. Singer, B.D., Mock, J.R., Aggarwal, N.R., Garibaldi, B.T., Sidhaye, V.K., Florez, M.A., Chau, E., Gibbs, K.W., Mandke, P., Tripathi, A., et al. (2015). Regulatory T Cell DNA Methyltransferase Inhibition Accelerates Resolution of Lung Inflammation. Am. J. Respir. Cell Mol. Biol. *52*, 641–652. https://doi.org/10.1165/rcmb.2014-0327OC.

51. Weinberg, S.E., Singer, B.D., Steinert, E.M., Martinez, C.A., Mehta, M.M., Martínez-Reyes, I., Gao, P., Helmin, K.A., Abdala-Valencia, H., Sena, L.A., et al. (2019). Mitochondrial complex III is essential for suppressive function of regulatory T cells. Nature *565*, 495–499. https://doi.org/10.1038/s41586-018-0846-z.

52. Workman, C.J., Collison, L.W., Bettini, M., Pillai, M.R., Rehg, J.E., and Vignali, D.A.A. (2011). In Vivo Treg Suppression Assays. Methods Mol. Biol. *707*, 119–156. https://doi.org/10.1007/978-1-61737-979-6_9.

53. Komatsu, N., Okamoto, K., Sawa, S., Nakashima, T., Oh-hora, M., Kodama, T., Tanaka, S., Bluestone, J.A., and Takayanagi, H. (2014). Pathogenic conversion of Foxp3 + T cells into T H 17 cells in autoimmune arthritis. Nat. Med. *20*, 62–68. https://doi.org/10.1038/nm.3432.

54. Constantinescu, C.S., Farooqi, N., O'Brien, K., and Gran, B. (2011). Experimental autoimmune encephalomyelitis (EAE) as a model for multiple sclerosis (MS). Br. J. Pharmacol. *164*, 1079–1106. https://doi.org/10.1111/j.1476-5381.2011.01302.x.

55. ROBINSON, A.P., HARP, C.T., NORONHA, A., and MILLER, S.D. (2014). The experimental autoimmune encephalomyelitis (EAE) model of MS: utility for understanding disease pathophysiology and treatment. Handb. Clin. Neurol. *122*, 173–189. https://doi.org/10.1016/B978-0-444-52001-2.00008-X.

56. Bailey-Bucktrout, S.L., Martinez-Llordella, M., Zhou, X., Anthony, B., Rosenthal, W., Luche, H., Fehling, H.J., and Bluestone, J.A. (2013). Self-antigen driven activation induces instability of regulatory T cells during an inflammatory autoimmune response. Immunity *39*, 949–962. https://doi.org/10.1016/j.immuni.2013.10.016.

57. Oh, D.Y., Kwek, S.S., Raju, S.S., Li, T., McCarthy, E., Chow, E., Aran, D., Ilano, A., Pai, C.-C.S., Rancan, C., et al. (2020). Intratumoral CD4+ T Cells Mediate Anti-tumor Cytotoxicity in Human Bladder Cancer. Cell *181*, 1612–1625.e13. https://doi.org/10.1016/j.cell.2020.05.017.

58. Wang, Y., Su, M.A., and Wan, Y.Y. (2011). An essential role of the transcription factor GATA-3 for the function of regulatory T cells. Immunity *35*, 337–348. https://doi.org/10.1016/j.immuni.2011.08.012.

59. Schmitt, E.G., Haribhai, D., Williams, J.B., Aggarwal, P., Jia, S., Charbonnier, L.-M., Yan, K., Lorier, R., Turner, A., Ziegelbauer, J., et al. (2012). IL-10 produced by iTreg cells controls colitis and pathogenic ex-iTreg cells during immunotherapy. J. Immunol. *189*, 5638–5648. https://doi.org/10.4049/jimmunol.1200936.

60. Kaiser, K.A., Loffredo, L.F., Santos-Alexis, K.d.L., Ringham, O.R., and Arpaia, N. (2023). Regulation of the alveolar regenerative niche by amphiregulin-producing regulatory T cells. J. Exp. Med. *220*, e20221462. https://doi.org/10.1084/jem.20221462.

61. Kurtulus, S., Sakuishi, K., Ngiow, S.-F., Joller, N., Tan, D.J., Teng, M.W.L., Smyth, M.J., Kuchroo, V.K., and Anderson, A.C. (2015). TIGIT predominantly regulates the immune response via regulatory T cells. J. Clin. Invest. *125*, 4053–4062. https://doi.org/10.1172/JCI81187.

62. Whiteside, S.K., Grant, F.M., Gyori, D.S., Conti, A.G., Imianowski, C.J., Kuo, P., Nasrallah, R., Sadiyah, F., Lira, S.A., Tacke, F., et al. (2021). CCR8 marks highly suppressive Treg cells within tumours but is dispensable for their accumulation and suppressive function. Immunology *163*, 512–520. https://doi.org/10.1111/imm.13337.

63. Kidani, Y., Nogami, W., Yasumizu, Y., Kawashima, A., Tanaka, A., Sonoda, Y., Tona, Y., Nashiki, K., Matsumoto, R., Hagiwara, M., et al. (2022). CCR8-targeted specific depletion of clonally expanded Treg cells in tumor tissues evokes potent tumor immunity with long-lasting memory. Proc. Natl. Acad. Sci. USA *119*, e2114282119. https://doi.org/10.1073/pnas.2114282119.

64. Van Damme, H., Dombrecht, B., Kiss, M., Roose, H., Allen, E., Van Overmeire, E., Kancheva, D., Martens, L., Murgaski, A., Bardet, P.M.R., et al. (2021). Therapeutic depletion of CCR8+ tumor-infiltrating regulatory T cells elicits antitumor immunity and synergizes with anti-PD-1 therapy. J. Immunother. Cancer *9*, e001749. https://doi.org/10.1136/jitc-2020-001749.

65. Tirosh, I., Izar, B., Prakadan, S.M., Wadsworth, M.H., Treacy, D., Trombetta, J.J., Rotem, A., Rodman, C., Lian, C., Murphy, G., et al. (2016). Dissecting the multicellular ecosystem of metastatic melanoma by single-cell RNA-seq. Science *352*, 189–196. https://doi.org/10.1126/science.aad0501.

66. Trapnell, C., Cacchiarelli, D., Grimsby, J., Pokharel, P., Li, S., Morse, M., Lennon, N.J., Livak, K.J., Mikkelsen, T.S., and Rinn, J.L. (2014). The dynamics and regulators of cell fate decisions are revealed by pseudotemporal ordering of single cells. Nat. Biotechnol. *32*, 381–386. https://doi.org/10.1038/nbt.2859.

67. Miyara, M., Yoshioka, Y., Kitoh, A., Shima, T., Wing, K., Niwa, A., Parizot, C., Taflin, C., Heike, T., Valeyre, D., et al. (2009). Functional Delineation and Differentiation Dynamics of Human CD4+ T Cells Expressing the FoxP3 Transcription Factor. Immunity *30*, 899–911. https://doi.org/10.1016/j.immuni.2009.03.019.

68. Finak, G., McDavid, A., Yajima, M., Deng, J., Gersuk, V., Shalek, A.K., Slichter, C.K., Miller, H.W., McElrath, M.J., Prlic, M., et al. (2015). MAST: a flexible statistical framework for assessing transcriptional changes and characterizing heterogeneity in single-cell RNA sequencing data. Genome Biol. *16*, 278. https://doi.org/10.1186/s13059-015-0844-5.

69. Subramanian, A., Tamayo, P., Mootha, V.K., Mukherjee, S., Ebert, B.L., Gillette, M.A., Paulovich, A., Pomeroy, S.L., Golub, T.R., Lander, E.S., and Mesirov, J.P. (2005). Gene set enrichment analysis: A knowledge-based approach for interpreting genome-wide expression profiles. Proc. Natl. Acad. Sci. USA *102*, 15545–15550. https://doi.org/10.1073/pnas.0506580102.

70. Heinz, S., Benner, C., Spann, N., Bertolino, E., Lin, Y.C., Laslo, P., Cheng, J.X., Murre, C., Singh, H., and Glass, C.K. (2010). Simple combinations of lineage-determining transcription factors prime cis-regulatory elements required for macrophage and B cell identities. Mol. Cell *38*, 576–589. https://doi.org/10.1016/j.molcel.2010.05.004.

71. Yuan, C.X., Ito, M., Fondell, J.D., Fu, Z.Y., and Roeder, R.G. (1998). The TRAP220 component of a thyroid hormone receptor- associated protein (TRAP) coactivator complex interacts directly with nuclear receptors in a

ligand-dependent fashion. Proc. Natl. Acad. Sci. USA *95*, 7939–7944. https://doi.org/10.1073/pnas.95.14.7939.

72. Llopis, J., Westin, S., Ricote, M., Wang, Z., Cho, C.Y., Kurokawa, R., Mullen, T.M., Rose, D.W., Rosenfeld, M.G., Tsien, R.Y., and Glass, C.K. (2000). Ligand-dependent interactions of coactivators steroid receptor coactivator-1 and peroxisome proliferator-activated receptor binding protein with nuclear hormone receptors can be imaged in live cells and are required for transcription. Proc. Natl. Acad. Sci. USA *97*, 4363–4368. https://doi.org/10.1073/pnas.97.8.4363.
73. Parang, B., Barrett, C.W., and Williams, C.S. (2016). AOM/DSS Model of Colitis-Associated Cancer. Methods Mol. Biol. *1422*, 297–307. https://doi.org/10.1007/978-1-4939-3603-8_26.
74. Loo, C.-S., Gatchalian, J., Liang, Y., Leblanc, M., Xie, M., Ho, J., Venkatraghavan, B., Hargreaves, D.C., and Zheng, Y. (2020). A Genome-wide CRISPR Screen Reveals a Role for the Non-canonical Nucleosome-Remodeling BAF Complex in Foxp3 Expression and Regulatory T Cell Function. Immunity *53*, 143–157.e8. https://doi.org/10.1016/j.immuni.2020.06.011.
75. Neumann, C., Blume, J., Roy, U., Teh, P.P., Vasanthakumar, A., Beller, A., Liao, Y., Heinrich, F., Arenzana, T.L., Hackney, J.A., et al. (2019). c-Maf-dependent Treg cell control of intestinal TH17 cells and IgA establishes host–microbiota homeostasis. Nat. Immunol. *20*, 471–481. https://doi.org/10.1038/s41590-019-0316-2.
76. Wheaton, J.D., Yeh, C.-H., and Ciofani, M. (2017). c-Maf is required for regulatory T cells to adopt RORγt+ and follicular phenotypes. J. Immunol. *199*, 3931–3936. https://doi.org/10.4049/jimmunol.1701134.
77. Mair, F., Erickson, J.R., Frutoso, M., Konecny, A.J., Greene, E., Voillet, V., Maurice, N.J., Rongvaux, A., Dixon, D., Barber, B., et al. (2022). Extricating human tumour immune alterations from tissue inflammation. Nature *605*, 728–735. https://doi.org/10.1038/s41586-022-04718-w.
78. Li, C., DiSpirito, J.R., Zemmour, D., Spallanzani, R.G., Kuswanto, W., Benoist, C., and Mathis, D. (2018). TCR Transgenic Mice Reveal Stepwise, Multi-site Acquisition of the Distinctive Fat-Treg Phenotype. Cell *174*, 285–299.e12. https://doi.org/10.1016/j.cell.2018.05.004.
79. Dikiy, S., Levine, A.G., Pritykin, Y., Krishna, C., Glasner, A., Leslie, C.S., and Rudensky, A.Y. (2022). Terminal differentiation and persistence of effector regulatory T cells essential for the prevention of intestinal inflammation. Preprint at bioRxiv. https://doi.org/10.1101/2022.05.16.492030.
80. Belakavadi, M., Pandey, P.K., Vijayvargia, R., and Fondell, J.D. (2008). MED1 Phosphorylation Promotes Its Association with Mediator: Implications for Nuclear Receptor Signaling. Mol. Cell Biol. *28*, 3932–3942. https://doi.org/10.1128/MCB.02191-07.
81. Rasool, R.U., Natesan, R., Deng, Q., Aras, S., Lal, P., Sander Effron, S., Mitchell-Velasquez, E., Posimo, J.M., Carskadon, S., Baca, S.C., et al. (2019). CDK7 inhibition suppresses Castration-Resistant Prostate Cancer through MED1 inactivation. Cancer Discov. *9*, 1538–1555. https://doi.org/10.1158/2159-8290.CD-19-0189.
82. Marineau, J.J., Hamman, K.B., Hu, S., Alnemy, S., Mihalich, J., Kabro, A., Whitmore, K.M., Winter, D.K., Roy, S., Ciblat, S., et al. (2022). Discovery of SY-5609: A Selective, Noncovalent Inhibitor of CDK7. J. Med. Chem. *65*, 1458–1480. https://doi.org/10.1021/acs.jmedchem.1c01171.
83. Sava, G.P., Fan, H., Coombes, R.C., Buluwela, L., and Ali, S. (2020). CDK7 inhibitors as anticancer drugs. Cancer Metastasis Rev. *39*, 805–823. https://doi.org/10.1007/s10555-020-09885-8.
84. Kwiatkowski, N., Zhang, T., Rahl, P.B., Abraham, B.J., Reddy, J., Ficarro, S.B., Dastur, A., Amzallag, A., Ramaswamy, S., Tesar, B., et al. (2014). Targeting transcription regulation in cancer with a covalent CDK7 inhibitor. Nature *511*, 616–620. https://doi.org/10.1038/nature13393.
85. Laaker, C., Hsu, M., Fabry, Z., Miller, S.D., and Karpus, W.J. (2021). Experimental Autoimmune Encephalomyelitis in the Mouse. Curr. Protoc. *1*, e300. https://doi.org/10.1002/cpz1.300.
86. Manglani, M., Gossa, S., and McGavern, D.B. (2018). Leukocyte Isolation from Brain, Spinal Cord, and Meninges for Flow Cytometric Analysis. Curr. Protoc. Im. *121*, e44. https://doi.org/10.1002/cpim.44.
87. Hao, Y., Hao, S., Andersen-Nissen, E., Mauck, W.M., Zheng, S., Butler, A., Lee, M.J., Wilk, A.J., Darby, C., Zager, M., et al. (2021). Integrated analysis of multimodal single-cell data. Cell *184*, 3573–3587.e29. https://doi.org/10.1016/j.cell.2021.04.048.
88. Choudhary, S., and Satija, R. (2022). Comparison and evaluation of statistical error models for scRNA-seq. Genome Biol. *23*, 27. https://doi.org/10.1186/s13059-021-02584-9.
89. Marsh, S., Tang, M., Kozareva, V., and Graybuck, L. (2023). scCustomize: Custom Visualizations & Functions for Streamlined Analyses of Single Cell Sequencing Version 1.1.1.
90. Zheng, Y., Josefowicz, S.Z., Kas, A., Chu, T.-T., Gavin, M.A., and Rudensky, A.Y. (2007). Genome-wide analysis of Foxp3 target genes in developing and mature regulatory T cells. Nature *445*, 936–940. https://doi.org/10.1038/nature05563.
91. Cooper, H.S., Murthy, S.N., Shah, R.S., and Sedergran, D.J. (1993). Clinicopathologic study of dextran sulfate sodium experimental murine colitis. Lab. Invest. *69*, 238–249.
92. Langmead, B., and Salzberg, S.L. (2012). Fast gapped-read alignment with Bowtie 2. Nat. Methods *9*, 357–359. https://doi.org/10.1038/nmeth.1923.
93. Feng, J., Liu, T., Qin, B., Zhang, Y., and Liu, X.S. (2012). Identifying ChIP-seq enrichment using MACS. Nat. Protoc. *7*, 1728–1740. https://doi.org/10.1038/nprot.2012.101.
94. Quinlan, A.R., and Hall, I.M. (2010). BEDTools: a flexible suite of utilities for comparing genomic features. Bioinformatics *26*, 841–842. https://doi.org/10.1093/bioinformatics/btq033.
95. Anders, S., Pyl, P.T., and Huber, W. (2015). HTSeq–a Python framework to work with high-throughput sequencing data. Bioinformatics *31*, 166–169. https://doi.org/10.1093/bioinformatics/btu638.
96. Love, M.I., Huber, W., and Anders, S. (2014). Moderated estimation of fold change and dispersion for RNA-seq data with DESeq2. Genome Biol. *15*, 550. https://doi.org/10.1186/s13059-014-0550-8.

STAR★METHODS

KEY RESOURCES TABLE

REAGENT or RESOURCE	SOURCE	IDENTIFIER
Antibodies		
anti-MED1	Cell Signaling Technologies	#51613
anti-GAPDH	Cell Signaling Technologies	#5174
blocking CD16/32 antibody	BioLegend	#101301
BV785 CD4(GK1.5)	BioLegend	#100453
BUV563 CD4(GK1.5)	Becton Dickinson	#612923
BV510 CD8(53–6.7)	BioLegend	#100751
BUV805 CD8(53–6.7)	Becton Dickinson	#612898
BUV CD45(30-F11)	Becton Dickinson	#564279
PerCP/Cy5.5 CD45(QA17A26)	BioLegend	#157612
PE CD25(A18246A)	BioLegend	#113704
APC/Cy7 CD44(IM7)	BioLegend	#103028
PE/Cy7 CD62L(MEL-14)	BioLegend	#104418
APC CD45.1(A20)	BioLegend	#110714
PerCP/Cy5.5 CD45.2(104)	BioLegend	#109828
PerCP/Cy5.5 CD45RB (C363-16A)	BioLegend	#103314
PerCP/Cy5.5 IL-7Ra(A7R34)	BioLegend	#135022
BV421 CCR7(4B12)	BioLegend	#120120
PE/Cy7 TIGIT(1G9)	BioLegend	#142108
APC-eFluor 780 ICOS(C398.4A)	Thermofisher Scientific	#47-9949-82
APC GITR(DTA-1)	BioLegend	#126312
FITC FOXP3 (FJK-16s)	Thermofisher Scientific	#11-5773-82
PE/Cy7 IFNγ (XMG1.2)	BioLegend	#505826
PE IL17A(TC11-18H10.1)	BioLegend	#506904
APC GM-CSF(MP1-22E9)	BioLegend	#505414
APC IRF8(V3GYWCH)	Thermofisher Scientific	#17-9852-82
Pacific Blue IRF4(IRF4.3E4)	BioLegend	#646418
APC/Cy7 HELIOS(22F6)	BioLegend	#137236
R718 TCF-1(S33-966)	Becton Dickinson	#567587
CD8 depleting antibody	Bio X Cell	#53–6.72
Isotype control	Bio X Cell	#2A3
Bacterial and virus strains		
mouse-adapted influenza A virus (A/WSN/33 [H1N1]	Dr. Benjamin D. Singer	N/A
Chemicals, peptides, and recombinant proteins		
Tamoxifen	Millipore Sigma	#T5648
Cell Trace Violet	Thermofisher Scientific	#C34557
RPMI	Cytiva	#SH30255.02
CD3/CD28 activation beads	Miltenyi Biotec	#130-095-925
Fetal Bovine Serum	R&D Systems	#S11150
Mouse IL2	PeproTech	#212-12
Penicillin/Streptomycin	Thermofisher Scientific	#15140122
$MOG^{20,35–54}$ peptide	EZ Biolabs	#cp7203
Freund's Complete Adjuvant	Santa Cruz Biotechnologies	#sc-24018
Pertussis toxin	List Biologicals	#180

(*Continued on next page*)

Continued

REAGENT or RESOURCE	SOURCE	IDENTIFIER
Azoxymethane	Millipore Sigma	#A5486
Dextran sodium sulfate	Thermofisher Scientific	#611361000
RIPA Buffer	Millipore Sigma	#20-188
protease inhibitors	Millipore Sigma	#4693132001
Laemmli sample buffer	Thermofisher Scientific	#A32957
Fixable Viability Dye eFluor 450	Thermofisher Scientific	#65-0863-18
Fixable Viability Dye eFluor 506	Thermofisher Scientific	#65-0866-14
Fixable Viability Dye eFluor 660	Thermofisher Scientific	#65-0864-14
Fixable Viability Dye eFluor 455UV	Thermofisher Scientific	#65-0868-14
Phorbol 12-myristate 13-acetate	Millipore Sigma	P8139
Ionomycin	Millipore Sigma	I9657
Monensin	BioLegend	420701
Collagenase type 4	Worthington Biochemical	# LS004189
HBSS	Thermofisher Scientific	#14170120
Ficoll-Paque	Millipore Sigma	#GE17-5446-02
Percoll	Cytiva	#17089101
10% formalin	Millipore Sigma	#HT501128-4L
TDE1 enzyme	Illumina	#20034197
Critical commercial assays		
$CD8^+$ T cell negative selection kit (mouse)	Stem Cell Technologies	Cat#19853
$CD4^+$ T cell negative selection kit (mouse)	Stem Cell Technologies	Cat#19765
Lamina propria dissociation kit (mouse)	Miltenyi Biotec	#130-097-410)
$CD45^+$ TIL isolation kit (mouse)	Stem Cell Technologies	#100-0350
Dead cell removal kit (mouse)	Stem Cell Technologies	#17899)
$CD4^+$ selection kit II (mouse)	Stem Cell Technologies	#18952
DNA Clean and Concentrator-5	Zymo Research	D4004
Deposited data		
scRNA-sequencing data (RM1 Intratumoral T regulatory cells)	This manuscript	GSE237966
ATAC-sequencing data (Splenic and RM1 Intratumoral T regulatory cells)	This manuscript	GSE237966
scRNA-sequencing data (Colitis and Colitis-associated cancer T regulatory cells)	This manuscript	GSE237966
Human oral mucosa and head and neck squamous cell carcinoma	Yuan et al.[71]	GSE163633
Experimental models: Cell lines		
B16-F10 Melanoma	ATCC	#CRL-6475
RM1 Prostate Cancer Cells	ATCC (Dr. Jindan Yu)	#CRL-3310
EG7 Lymphoma	Dr. Bin Zhang	N/A
Foxp3/Transcription Factor Staining Buffer Set	Thermofisher Scientific	#00-5523-00
Experimental models: Organisms/strains		
Foxp3$^{YFP-cre}$ mice	Jackson Laboratory	stock no. 016959
Foxp3$^{eGFP-CreERT2}$ mice	Jackson Laboratory	stock no. 016961
ROSA26Sor$^{CAG-tdTomato}$ mice	Jackson Laboratory	stock no. 007908
Med1$^{fl/fl}$ mice	Janardan K. Reddy[29]	N/A
Rag1^{tm1Mom} mice	Jackson Laboratory	stock no. 002216
B6.SJL-*Ptprc*^{a} *Pepc*^{b}/BoyJ mice	Jackson Laboratory	stock no. 007908
Software and algorithms		
FlowJo v10	Becton Dickinson	https://www.flowjo.com/
Seurat v4.2.1	Sava et al.[83]	https://satijalab.org/seurat/

(*Continued on next page*)

Continued

REAGENT or RESOURCE	SOURCE	IDENTIFIER
R v4.1.0	Cran Project	https://cran.r-project.org/bin/windows/base/
SCTransform V2	Kwiatkowski et al.[84]	https://satijalab.org/seurat/articles/sctransform_v2_vignette.html
MAST v1.24	Whiteside et al.[62]	https://bioconductor.org/packages/release/bioc/html/MAST.html
scCustomize v1.1.1	Laaker et al.[85]	https://samuel-marsh.github.io/scCustomize/
Monocle v3	Schmitt et al.[59]	https://cole-trapnell-lab.github.io/monocle3/
Gene set enrichment analysis v4.2.3	Kidani et al.[63]	http://www.gsea-msigdb.org/gsea/index.jsp
Cell Ranger	10X Genomics	https://www.10xgenomics.com/
Bowtie v2	Manglani et al.[86]	https://bowtie-bio.sourceforge.net/bowtie2/index.shtml
MACS2	Hao et al.[87]	https://github.com/macs3-project/MACS
Bedtools v2.28	Choudhary and Satija[88]	https://bedtools.readthedocs.io/en/latest/
HTSeq-count 0.11.1	Marsh et al.[89]	https://htseq.readthedocs.io/en/release_0.11.1/count.html
DESeq2	Zheng et al.[90]	https://bioconductor.org/packages/release/bioc/html/DESeq2.html
HOMERv4.11	Van Damme et al.[64]	http://homer.ucsd.edu/homer/
Prism v9	Graphpad	https://www.graphpad.com/scientific-software/prism/
Other		
PAGE gels	BioRad	#4561085

RESOURCE AVAILABILITY

Lead contact

Further information and requests for resources and reagents should be directed to and will be fulfilled by the lead contact, Deyu Fang (fangd@northwestern.edu).

Materials availability

No new materials were generated during this work. Mice generated are available upon request. Direct requests to Deyu Fang (fangd@northwestern.edu).

Data and code availability

- Bulk RNA-sequencing, Single cell RNA-sequencing and ATAC-sequencing data are deposited in the Gene Expression Omnibus. Accession number: GSE237966.
- No novel code was generated during publication. Standard tools utilized are described in method details.
- All other data available upon request and fulfilled by lead author.

EXPERIMENTAL MODEL AND STUDY PARTICIPANT DETAILS

Mice

Med1 floxed mice were a kind gift from Dr. Janardhan K. Reddy and generated as described previously.[39] *Foxp3*$^{YFP-cre}$ (stock no. 016959), *Foxp3*$^{eGFP-CreERT2}$ (stock no. 016961), and *ROSA26Sor*$^{CAG-tdTomato}$ (Ai14, stock no. 007908) mice were obtained from The Jackson Laboratory. Constitutive T Regulatory (T_{reg}) cell knockout mice (Med1$^{Treg-KO}$) were generated by crossing *Med1*$^{fl/fl}$ mice with *Foxp3*$^{YFP-cre}$ mice.

Inducible T_{reg} cell specific knockout mice (Med1$^{Treg-iKO}$) were generated by crossing *Med1*$^{fl/fl}$ with *Foxp3*$^{eGFP-CreERT2}$ and *ROSA26Sor*$^{CAG-tdTomato}$ mice. Deletion of MED1 was induced by oral gavage of 40 mg/ml tamoxifen (Millipore Sigma #T5648) in corn oil (Thermofisher Scientific # AC405435000) every 2-3 days to reach an effective dose of 320 mg/kg. Tamoxifen in corn oil was administered to both control and Med1$^{Treg-iKO}$ mice.

Rag1^{tm1Mom} lymphocyte deficient mice (stock no. 002216) and B6.SJL-*Ptprc*^{a} *Pepc*^{b}/BoyJ (stock no. 002014) were purchased from The Jackson Laboratory for adoptive transfer colitis experiments.

Unless otherwise noted, mice used for experiments were aged between 8 and 16 weeks, and equal proportions of males and females were used.

Animals received water *ad libitum*, were housed at a temperature range of 20°C–23°C under 12-h light/12-h dark cycles, and received standard rodent chow. These mice were maintained and used at the Northwestern University mouse facility under pathogen-free conditions in accordance with institutional guidelines and following animal study proposals approved by the institutional animal care and use committees (IACUC).

In vitro T regulatory cell suppression assay

$CD8^+$ T cells were enriched from spleens of C57BL/6J mice using a $CD8^+$ T cell negative selection kit (Stem Cell Technologies #19853) and then isolated through flow sorting. $CD4^+$ T_{reg} cells were enriched using a $CD4^+$ T cell negative selection kit (Stem Cell Technologies #19765) and then isolated through flow sorting. $CD8^+$ T cells were stained with Cell Trace Violet (Thermofisher Scientific #C34557) and then $2.5x10^4$ cells were plated per well in RPMI (Cytiva #SH30255.02) in a 96 well plate with $7.5x10^4$ CD3/CD28 activation beads (Miltenyi Biotec #130-095-925), 10% fetal bovine serum (FBS) (R&D Systems #S11150), and 30 IU/mL IL2 (PeproTech #212-12). Varying ratios of T_{reg} cells were incubated with $CD8^+$ T cells for 72 h and then CD8 T cell proliferation was measured by flow cytometry analysis of Cell Trace Violet dilution.[42]

Syngeneic tumor models, cell culture and tumor injections

B16-F10 melanoma cells (ATCC #CRL-6475) were purchased from ATCC. RM1 prostate cancer cells (ATCC #CRL-3310) were a generous gift from Dr. Jindan Yu. EG7 lymphoma cells were a kind gift from Dr. Bin Zhang. All cells were cultured in DMEM (Cytiva #SH30243.FS) with 10%FBS and 100U/ml Penicillin/Streptomycin (Thermofisher Scientific #15140122) at 5% CO_2 at 37°C. When cells reached 60–80% confluency, they were washed and resuspended in 100ul of phosphate-buffered saline (PBS), then injected subcutaneously into the right hind flanks of mice. $5x10^4$ cells B16-F10 cells, $5x10^4$ cells RM1 cells, and $1x10^5$ cells EG7 cells were injected per mouse. RM1 tumor experiments utilized only male mice as prostate cancer primarily affects men. Mice were monitored daily for tumor growth. Tumor volume was measured through digital calipers along three orthogonal axes (*x*, *y*, and *z*), and calculated as (*xyz*)/2. Mice were euthanized if tumors exceeded the 2500 mm^3 tumor size limit agreed by the Institutional Review Board (IRB). Specifically for Figure 2O, 2 mice exceeding this limit at day 17 were removed. The tumor sizes of each mouse in Figures 2A, 2B, 2C, 2F, and 2O are shown in Table S1.

T cell adoptive transfer colitis model

Naive T conventional (T_{conv}) cells ($CD4^+$ CD45.1+ CD45RB high $CD25^-$) were flow sorted from B6.SJL mice. T_{reg} cells were ($CD4^+$ CD45.2+ YFP+) were flow sorted from control and $Med1^{Treg-KO}$ mice. $4x10^5$ T_{conv} were retro-orbitally transferred alone or co-transferred with $1x10^5$ T_{reg} cells from either control or $Med1^{Treg-KO}$ mice into *Rag1*^{tm1Mom} recipient mice. Mice were measured weekly for body weight and monitored for clinical signs of colitis. Mice were sacrificed at 8 weeks once any group dropped 20% of body weight. Mesenteric lymph nodes were harvested for flow cytometry and colons were harvested for histology.[52]

Induced experimental autoimmune encephalomyelitis (EAE) model

Per mouse, 200ug of $MOG^{20,35-54}$ peptide (EZ Biolabs #cp7203) emulsified in Freund's Complete Adjuvant (Santa Cruz Biotechnologies #sc-24018). Mice were then subcutaneously injected with 150ul of the emulsification with 75ul each on the right and left flanks. Mice were then intraperitoneally injected with 200ng of pertussis toxin (List Biologicals #180) and then once again two days later. Mice were assessed daily for clinical signs of EAE. Scores were given as follows: 0, no sign of disease; 1, limp tail or hindlimb weakness but not both; 2, limp tail and hindlimb weakness; 3, partial hindlimb paralysis; 4, complete hindlimb paralysis; 5, Moribund state, euthanize mouse.[85] Evaluator was blinded to genotypes of mice.

Influenza model

Mice were anesthetized by intraperitoneal injection of 5% ketamine and 15% xylazine in 100ul of PBS. Mice were then intubated using a 20-gauge angiocatheter cut to a length that placed the tip of the catheter above the carina. Mice were instilled with 6.5 PFU of a mouse-adapted influenza A virus (A/WSN/33 [H1N1]) in 50ul PBS. Mice were measured every two days for body weight, heart rate, and oxygen saturation using the MouseOx Plus (STARR Life Sciences).

Colitis-associated-cancer model

Mice were intraperitoneally injected with a 100ul of Azoxymethane (Millipore Sigma #A5486) at 12.5 mg/kg in PBS. After 5 days mice were treated with 5 cycles of dextran sodium sulfate (Thermofisher Scientific #611361000) (DSS) at 3% in water followed by recovery (5 days DSS then 14 days water). Mice were monitored weekly for survival and disease activity index.[91] Mice were sacrificed at the peak of cycle 5 without recovery. Colons were extracted and analyzed for tumor number and size. Tumors were then digested for T_{reg} cell isolation.[73]

Dextran sodium sulfate (DSS) model

Mice were treated with 3% DSS in water for 6 days. Mice were monitored daily for body weight changes and clinical signs of colitis. On day 6 mouse stools were observed to calculate disease activity index.[91] Mice were then euthanized at peak of disease, colons

were used for histology, and lamina propria were digested for T_{reg} cell isolation.[73] Scoring was as follows 0, healthy colon; 1, minimal inflammation with minimal to no separation of crypts (generally focal affecting <10% of mucosa); 2, mild inflammation with mild separation of crypts (generally affecting 11%–25% of mucosa or mild, diffuse inflammatory infiltrates with minimal separation of crypts); 3, moderate inflammation with separation of crypts, with or without focal effacement of crypts (generally affecting 26%–50% of mucosa or moderate, diffuse separation of crypts); 4, extensive inflammation with marked separation and effacement of crypts (generally affecting >50% of mucosa). Lamina propria lymphocytes were isolated using a dissociation kit as per manufacturer's instructions (Miltenyi Biotec #130-097-410).

METHOD DETAILS

Isolation of lymphocytes from lymphoid organs

Mice were euthanized with CO_2 and cervical dislocation prior to isolation of lymphoid organs. Lymphoid organs were then mashed through a sterile 70uM nylon mesh filter. Samples were then spun down and treated with ACK lysis buffer (0.15M Ammonium chloride, 10mM Potassium bicarbonate, and 0.1mM Disodium EDTA) for 2 min. ACK lysis was then quenched with RPMI, cells were spun down and subjected to downstream analyses.

Protein extraction and western blot

Cells were lysed in RIPA buffer (Millipore Sigma #20–188) with 1X protease inhibitors (Millipore Sigma #4693132001) and 1X phosphatase inhibitors (Thermofisher Scientific #A32957) for 30 min at room temperature. Lysates were then centrifuged at x15,000G for 10 min and supernatants were collected. Lysates were then mixed with sample buffer (Thermofisher Scientific #A32957), heated at 95°C for 5 min, and loaded onto PAGE gels (BioRad #4561085). Gels were transferred to nitrocellulose membranes and blocked for 1 h in 5% milk. Membranes were then incubated with anti-MED1 (Cell Signaling Technologies #51613S at 1:1000) or anti-GAPDH (Cell Signaling Technologies #5174 at 1:1000) antibodies overnight and corresponding secondary antibodies for 1 h on the following day. Membranes were then imaged using the ChemiDoc imaging system (BioRad #ChemiDocXRS).

Flow cytometry analysis, intracellular cytokine stimulation, and cell sorting

Single cell suspensions were incubated with blocking CD16/32 antibody (BioLegend #101301) and then Fixable Viability Dye (ThermoFisher Scientific). All staining used 0.5-5x10^6 cells stained in 100ul 3% FBS in PBS with antibodies at manufacturer's recommendation unless otherwise specified. Antibodies included CD4(GK1.5), CD8(53–6.7), CD25(A18246A), CD44(IM7), CD62L(MEL-14), CD45(QA17A26), CD45.1(A20), CD45.2(104), CD45RB (C363-16A), IL7Ra(A7R34), CCR7(4B12), TIGIT(1G9), ICOS (C398.4A), and GITR(DTA-1). Surface-directed antibodies were stained for 20 min at 4°C then washed before analysis or intracellular staining. For detection of intracellular proteins, the Foxp3/Transcription Factor Staining Buffer Set (Thermofisher Scientific #00-5523-00) was used. Intracellular Antibodies included FOXP3 (FJK-16s), IFNγ (XMG1.2), IL17A(TC11-18H10.1), GM-CSF(MP1-22E9), IRF8 (V3GYWCH), IRF4(IRF4.3E4), HELIOS (22F6), TCF-1(S33-966). For samples requiring intracellular cytokine staining cells were first incubated for 4 h with 25 ng/mL PMA, 0.5uM ionomycin, and 10 μg/mL monensin. All analysis was performed on a BD LSRFortessa X-20 Analyzer and a BD FACSymphony A5-Laser Analyzer. All cell sorting was performed on BD SORP FACS Aria II or Miltenyi Tyto. All analysis was performed on FlowJo v10 (BD).

Isolation of tumor-infiltrating lymphocytes

Tumors were harvested from mice, weighed, and then minced into 1mm by 1mm pieces. Minced tumors were incubated with 2 mg/ml collagenase type 4 (Worthington Biochemical # LS004189), 5mM calcium chloride, and 1% FBS in HBSS (Thermofisher Scientific #14170120) at 37°C for 30–60 min. Tumors were then passed through an 18G needle onto a sterile 70uM nylon mesh filter. Samples then were subjected to red blood cell lysis with ACK lysis buffer. After single cell suspensions were obtained, cells were subjected to different enrichments based on downstream analyses required.

Prior to flow cytometry analysis most samples were subjected to density gradient centrifugation with Ficoll-Paque (Millipore Sigma #GE17-5446-02). Samples were diluted to 20mL, then 8mL of Ficoll-Paque was added below the cell suspension, samples were spun at x1000g for 20 min at 23°C with no breaks. Enriched cells were collected from the interphase of RPMI and Ficoll-Paque. For more sensitive downstream analyses target cells were enriched with either the $CD45^+$ TIL kit (Stemcell Technologies #100–0350), $CD4^+$ selection kit (Stemcell Technologies #18952), or dead cell removal kit (Stemcell Technologies #17899). Kits were used as per manufacturer's instructions.

CD8 T cell depletion

Mice were intraperitoneally treated with 200ug of CD8 depleting antibody (Bio X Cell #53–6.72) or isotype control (Bio X Cell# 2A3) in 100ul of PBS every 3 days starting on day 5.

Isolation of central nervous system (CNS) lymphocytes

CNS lymphocytes were isolated by the following protocol.[86] In brief, mice were perfused with saline, then brain, meninges, and spinal cord were collected in cold RPMI. Tissues were minced and digested in 2 mg/ml collagenase type 4 (Worthington Biochemical

LS004189) for 30 min at 37°C. Cells were then passed through a 100uM nylon mesh filter, pelleted, and resuspended in 90% Percoll (Cytiva #17089101). Samples were then overlayed with 60% Percoll, 40% Percoll, and HBSS, then centrifuged to obtain mononuclear cells.

Tissue fixation and histology

Mouse tissues were fixed in 10% formalin (Millipore Sigma #HT501128-4L) and embedded in paraffin. 4μm sections were stained with hematoxylin and eosin. The images were viewed on an Olympus CX31 microscope and taken with a PixelLink camera.

Single-cell RNA sequencing

Library preparation and sequencing

Single cell library preparation and sequencing was done at Northwestern University NUseq facility core with the support of NIH Grant (1S10OD025120). Cell number and viability of single cell suspension were analyzed using Nexcelom Cellometer Auto2000 with AOPI fluorescent staining method. Sixteen thousand cells were loaded into the Chromium Controller (10X Genomics, PN-120223) on a Chromium Next GEM Chip K (10X Genomics, PN-1000127), and processed to generate single cell gel beads in the emulsion (GEM) according to the manufacturer's protocol. The cDNA and library were generated using the Chromium Next GEM Single Cell 5′ Reagent Kits v2 (10X Genomics, PN-1000283) according to the manufacturer's manual. The multiplexed libraries were pooled and sequenced on Illumina Novaseq6000 sequencer with paired-end 50 kits using the following read length: 28 bp Read1 for cell barcode and UMI and 90 bp Read2 for transcript. The targeted sequencing depth for gene expression is 25,000 reads per cell.

Analysis

Raw sequencing data, in base call format (.bcl) was demultiplexed using Cell Ranger from 10x Genomics, converting the raw data into FASTQ format. Cell Ranger was also used for alignment of the FASTQ files to the mouse reference genome (mm10) and to count the number of reads from each cell that align to each gene, generating matrix files for each sample. Matrix files were analyzed using the Seurat R package (Seurat v4.2.1, R version 4.1.0).[87] Libraries were loaded individually and filtered based on the following metrics. Cells needed to have between 200 and 4,000 unique genes detected, less than 5% mitochondrial reads, less than 40% ribosomal reads, and less than 0.5% hemoglobin gene reads. Technical sources of variation were then accounted for by utilizing the SCTransform V2 package to normalize and integrate libraries.[88] PCA was performed on variable genes and 19 principal components were selected for UMAP construction and the FindNeighbhors tool. We performed FindClusters serially at different resolutions at settled at 0.4 to avoid over-segmentation. Differential gene expression between clusters and conditions was performed using the FindMarkers and FindAllMarkers functions with the Wilcoxon Test. Module scores were assigned using the AddModuleScore function. FetchData was then used to obtain module scores for individual cells and then Wilcoxon test was used to compare modules scores between different condition within clusters. Pseudobulk analysis between conditions was performed using the MAST package.[68] Additional visualization was performed with the scCustomize package.[89] Trajectory analysis and pseudotime ordering were performed using the Monocle package.[66] Graph test function was performed to calculate Morans' I for genes regulating specific trajectory within Monocle. Gene set enrichment analysis was performed using the GSEA prerank test function[69] and gene sets deposited from prior publication.[90]

Bulk RNA sequencing

Sequencing

RNA sequencing was performed by the Northwestern RNA sequencing core.

Analysis

The quality of DNA reads, in fastq format, was evaluated using FastQC. Adapters were trimmed, and reads of poor quality or those aligning to ribosomal RNA (rRNA) sequences were filtered. The cleaned reads were aligned to the Mus musculus genome (mm10) using STAR. Read counts for each gene were calculated using htseq-count in conjunction with a gene annotation file for mm10 obtained from UCSC (University of California Santa Cruz; http://genome.ucsc.edu). Differential expression was determined using edgeR. The cutoff for determining significantly differentially expressed genes was a false discovery rate (FDR)–adjusted p value of less than 0.05.

ATAC sequencing

Library preparation and sequencing

50,000 cells were washed in cold phosphate-buffered saline (PBS) to eliminate traces of DNase and buffer. Cell membrane was permeabilized with nuclear lysis buffer (10 mM tris, 10 mM NaCl, 3 mM MgCl2, and 0.5% IGEPAL-630). Then, cells were resuspended in 50uL of transposase reaction mixture (22.5uL nuclease-free water, 25uL of TD buffer and 2.5uL of TDE1 enzyme, Illumina #20034197). Transposition was carried out at 37°C for 22 min, followed by DNA purification with DNA Clean and Concentrator-5 (Zymo Research) according to the manufacturer's recommendation. Following purification, library fragments were PCR amplified with Nextera XT v2 adapter primers. Multiplexed and pooled library was sequencing on the NextSeq 500 (Illumina) with 37 nucleotides (nt) paired ends according to the manufacturer's instructions.

Analysis

Paired end ATACseq reads were aligned to the mouse genome (NCBI37/mm10) using Bowtie2[92] with option ''–very-sensitive-local''. Mitochondrial reads were excluded from downstream analysis. Peak calling was performed on each individual sample by MACS2[93] with parameter ''-BAMPE''. Peaks from different ATACseq replicates and samples were merged using bedtools merge.[94] Merged peaks were converted into GTF files and used for HTSeq-count.[95] Pairwise comparisons of ATACseq peaks between two conditions were performed using R package DESeq2[96] with reads count of each peak calculated by HTSeq-count. For tumor focused analysis, peaks from four replicates were merged and used for downstream analysis. Transcription start sites(TSS) of down-regulated genes were extended 10 kb or 50 kb in both directions. ATACseq peaks fall into those regions were identified using bedtools intersect.[94] Motif search was performed using Homer[70] script findMotifGenome.pl with parameter ''-size given''. Incidences of specific motif in the peaks were examined using Homer script annotatePeaks.pl with parameter ''-m -mbed'' set for that motif.

QUANTIFICATION AND STATISTICAL ANALYSIS

All statistical parameters are described in the figure legends. Sample size and definition of samples are defined in figure legends. In all figures, error bars represent SEM. Statistical analysis were performed within Prism v9. Statistical analyses related to single cell RNA-sequencing data were performed within R. Sample sizes were not predetermined. All experiments were replicated independently at least two times.